Cosmic Ray Studies at the Pierre Auger Observatory

Depth of maximum of air-shower profiles at the Pierre Auger Observatory. I. Measurements at energies above $10^{17.8}$ eV

A. Aab *et al.* (Pierre Auger Collaboration)
Phys. Rev. D **90**, 122005 – Published 31 December 2014

S. Paredes Saenz

on behalf of

The Maradona-Pelé Collaboration (work-in-progress name)

Overview

- Introduction & Motivation
- The Pierre Auger Observatory
- Data Selection
- Measurements & Results
- Summary & Conclusion

What are cosmic rays?

- **Energetic particles** from outer space
- **Primary particle** can be a charged **nucleus** or **gamma** rays
    - Primary interacts with the **atmosphere**, decaying into an **air shower**
    - Leptonic cascade is well modeled, hadronic is model-dependent

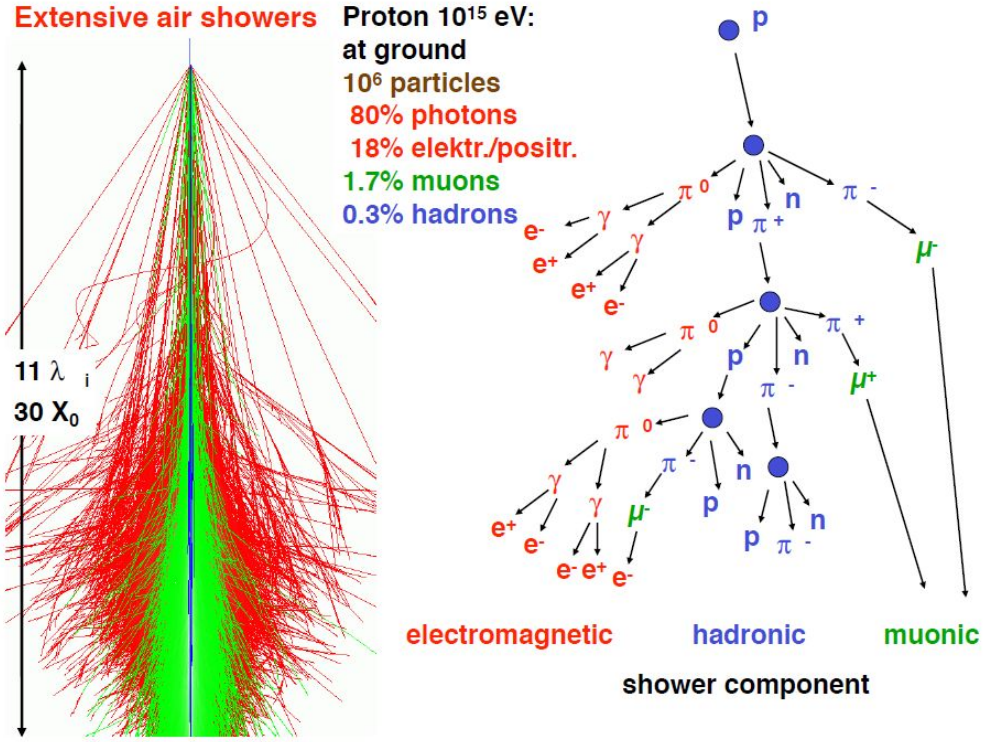

Why study them?

Why

SEARCH

NEW YORK POST

TECH

NASA worried that cosmic rays are going to fry plane passengers' brains

By Margi Murphy, The Sun

January 30, 2017 | 4:14pm | Updated

Why study them?

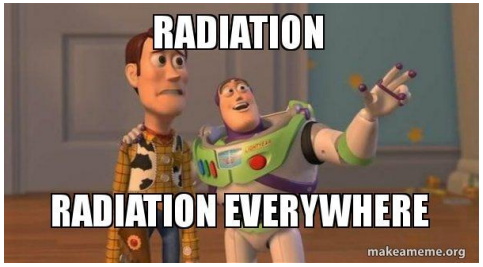

- What is the **origin** of cosmic rays?
  - Supernovae
  - Massive black holes
  - γ-ray bursters
  - Colliding galaxies
- They bring information of the chemical composition of the universe.

  What is their **mass composition**?

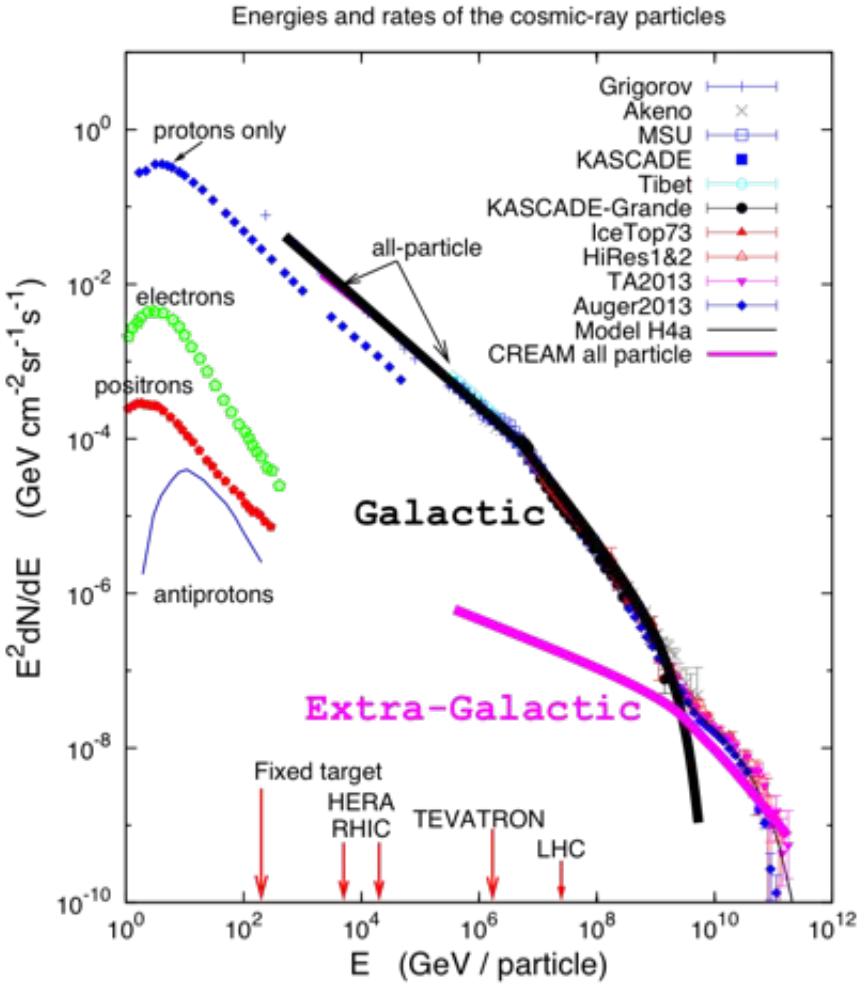

Problems

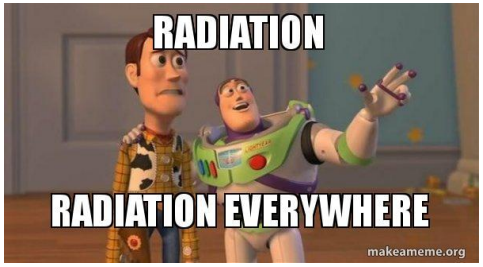

- Interplanetary travel, space probes, airplane jets, mobile phones, biological.

How can we study them?

- At high energies (> 10^{15} eV) only via **extensive air showers**.
  - Test of hadronic models and cross sections at **very high energies**

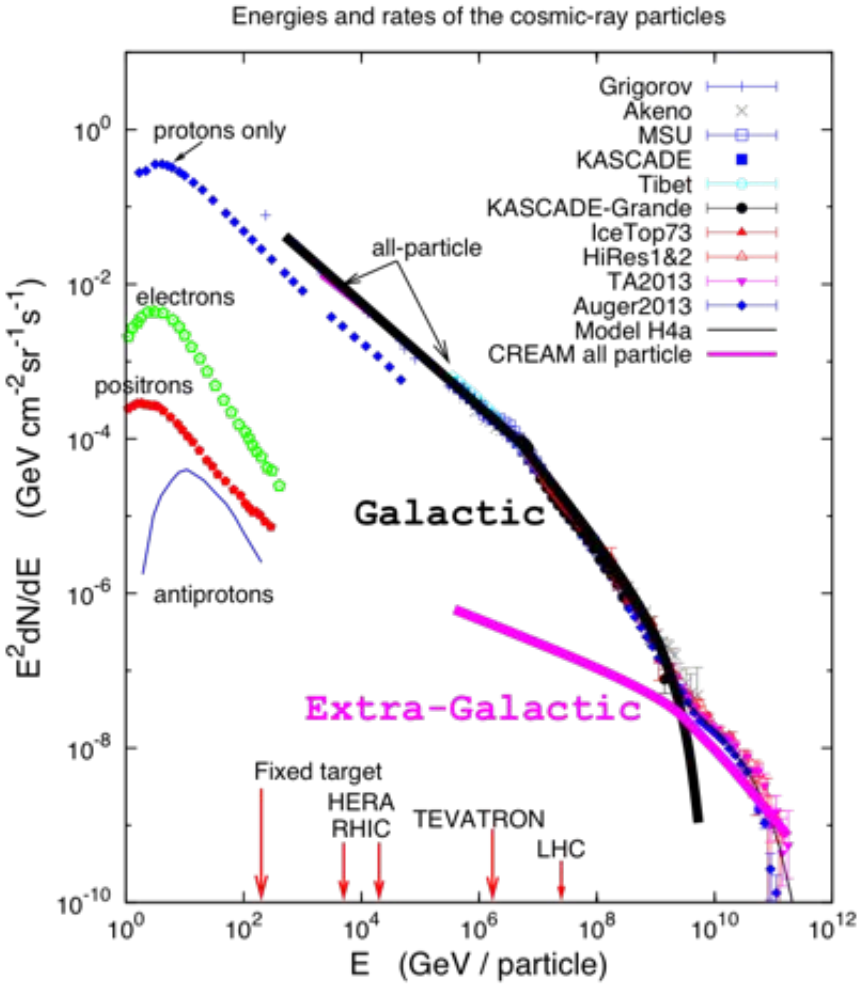

Problems

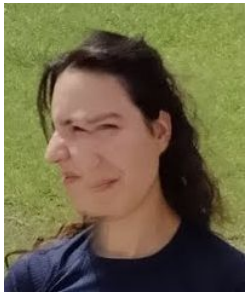

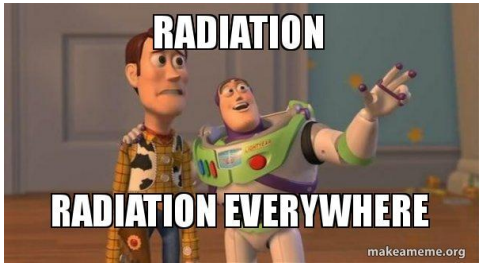

- Interplanetary travel, space probes, airplane jets, mobile phones, biological.

How can we study them?

- At high energies (> 10^{15} eV) only via **extensive air showers**.
  - Test of hadronic models and cross sections at **very high energies**

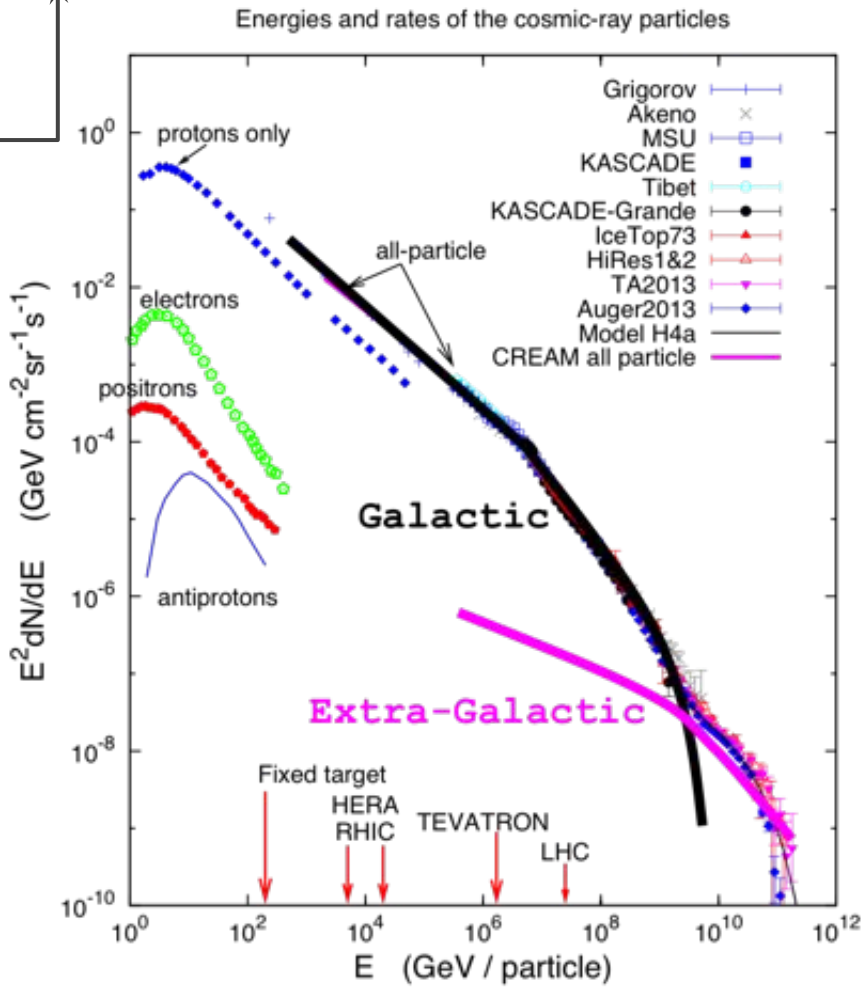

Problems

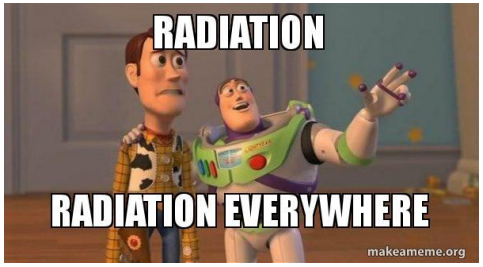

- Interplanetary travel, space probes, airplane jets, mobile phones, biological.

How can we study them?

- At high energies (> 10^{15} eV) only via **extensive air showers**.
  - Test of hadronic models and cross sections at **very high energies**

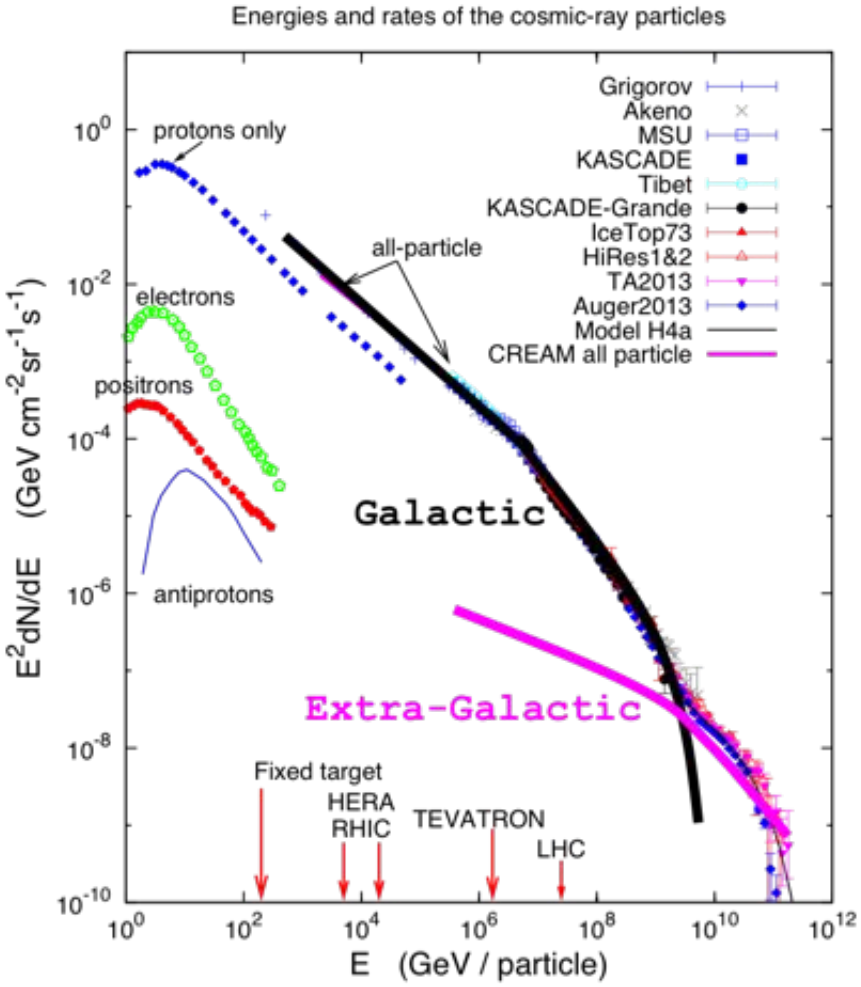

The Pierre Auger Observatory

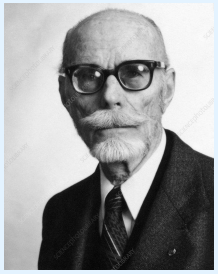

Pierre Auger Observatory

(Malargüe, Mendoza, Argentina)

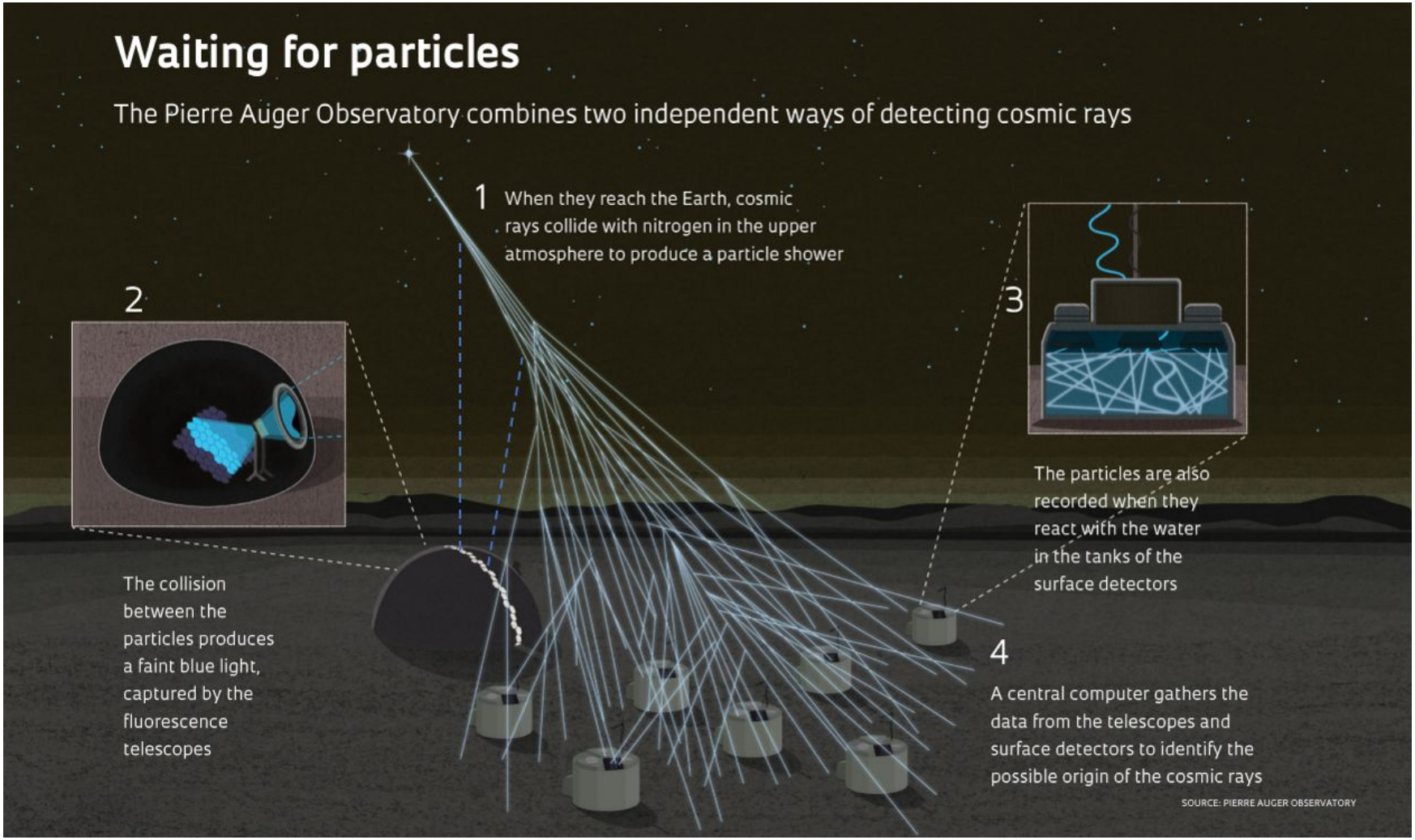

What do we measure?

Slant Depth

$$X(z) = \int_z^{\infty} \rho(\mathbf{r}(z'))dz'$$

→ **Amount of material traversed** by the shower at a z position on the shower axis.

$$X(z_{sea-level}) \sim 1000 \frac{g}{cm^2}$$

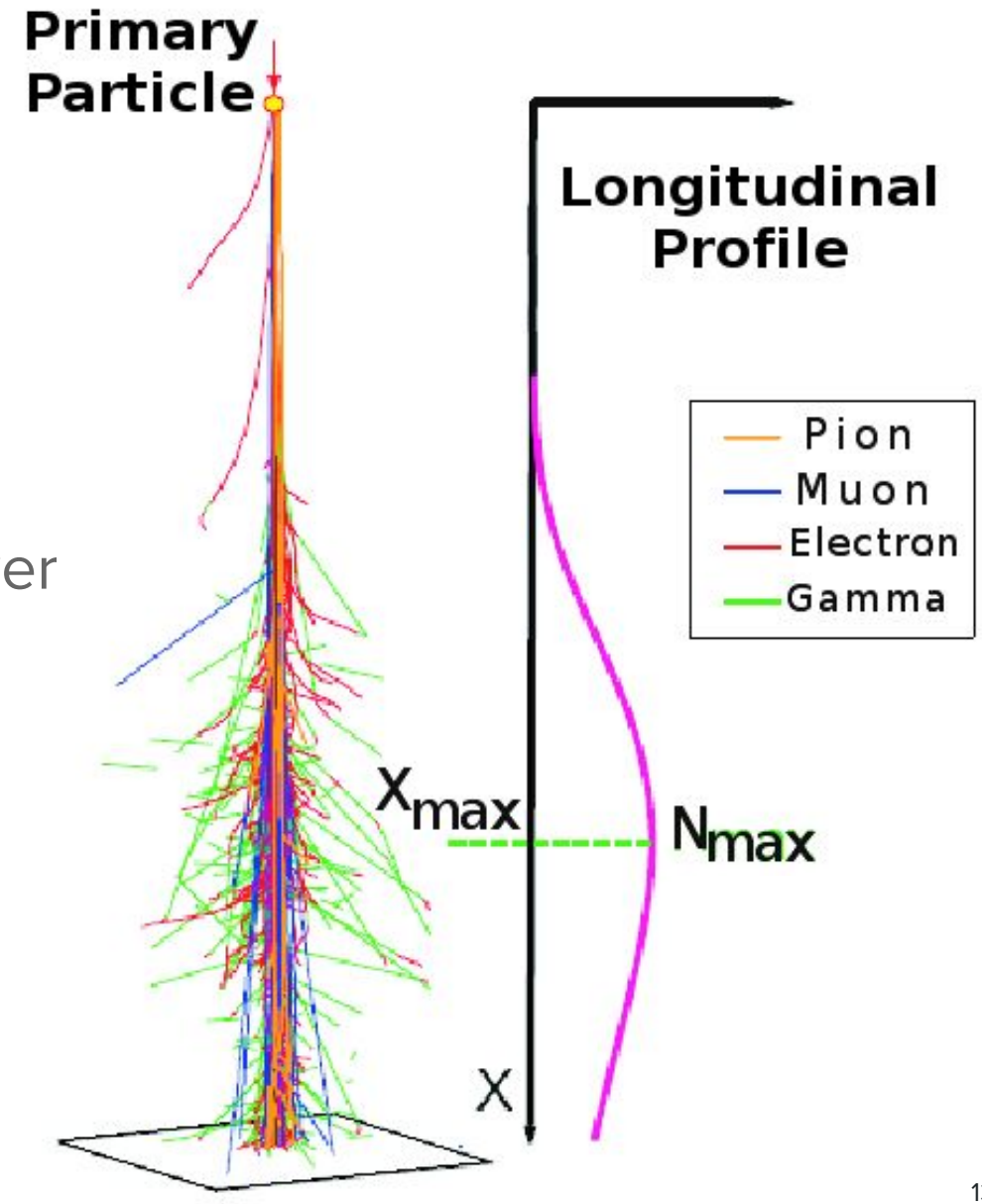

What do we measure?

Slant Depth

$$X(z) = \int_z^{\infty} \rho(\mathbf{r}(z'))dz'$$

→ **Amount of material traversed** by the shower at a z position on the shower axis.

$$X(z_{sea-level}) \sim 1000 \frac{g}{cm^2}$$

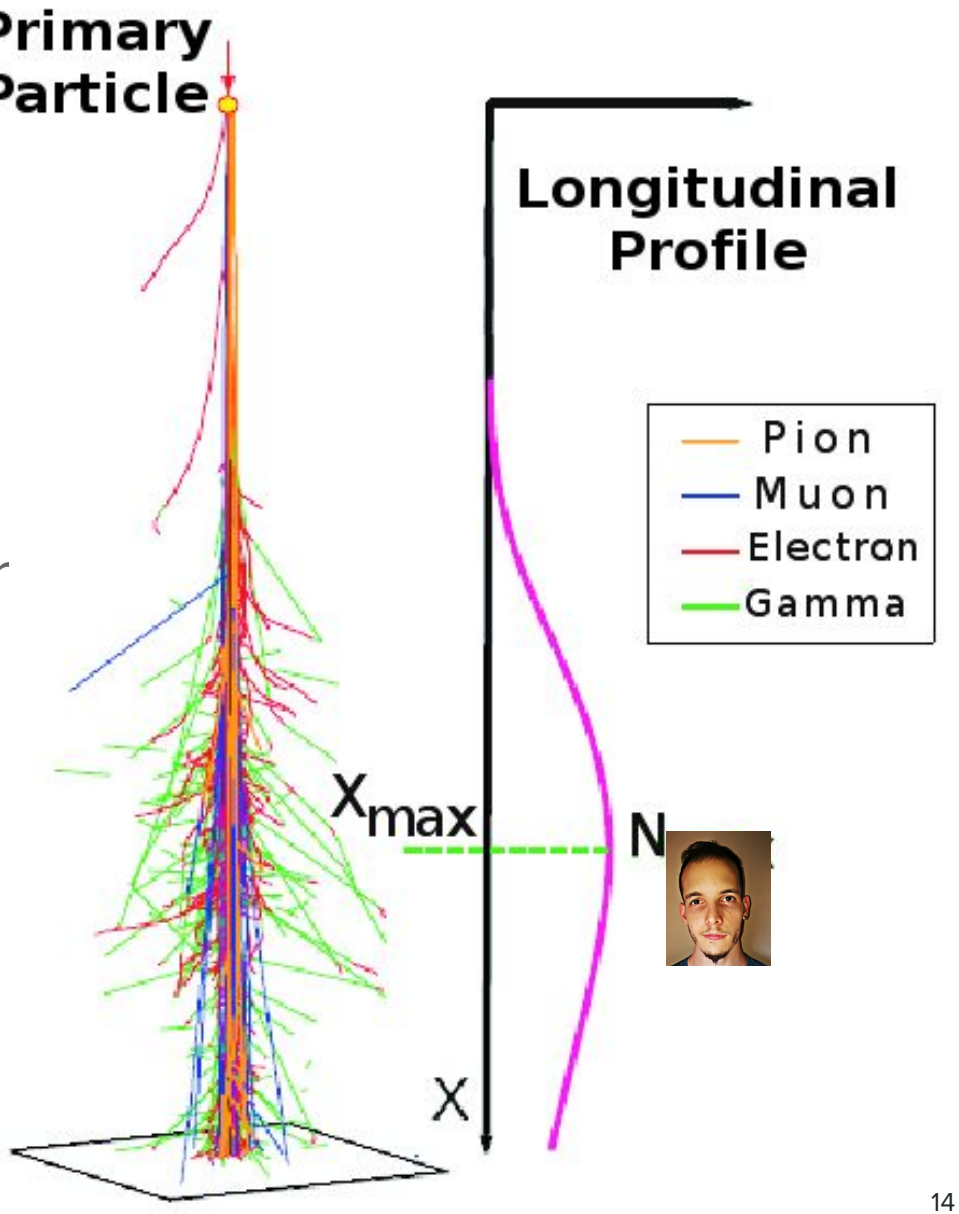

What do we measure?

Slant Depth

$$X(z) = \int_z^{\infty} \rho(\mathbf{r}(z'))dz'$$

→ **Amount of material traversed** by the shower at a z position on the shower axis.

$$X(z_{sea-level}) \sim 1000 \frac{g}{cm^2}$$

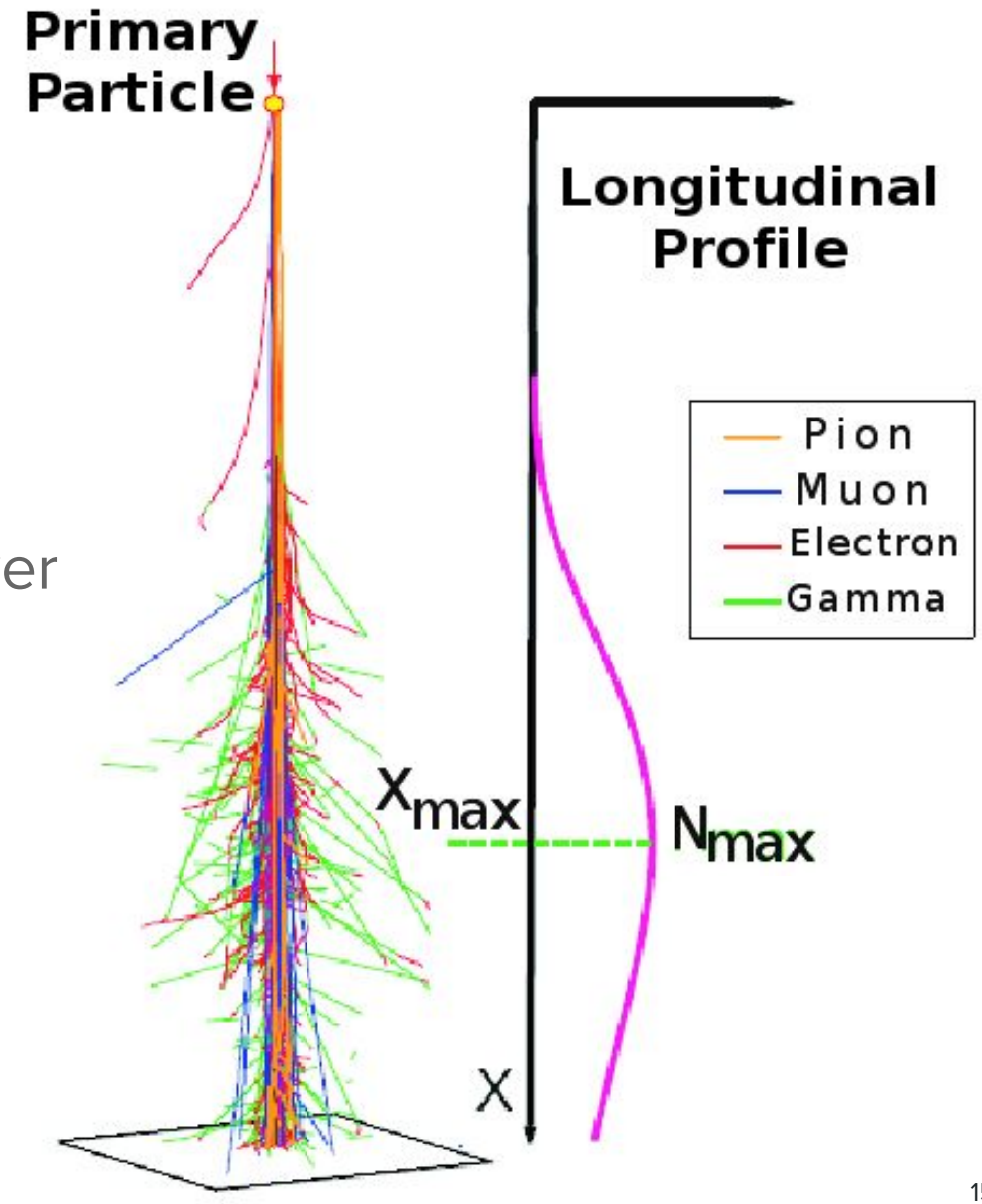

What do we measure?

Slant Depth

$$X(z) = \int_z^{\infty} \rho(\mathbf{r}(z'))dz'$$

→ **Amount of material traversed** by the shower at a z position on the shower axis.

$$X(z_{sea-level}) \sim 1000 \frac{g}{cm^2}$$

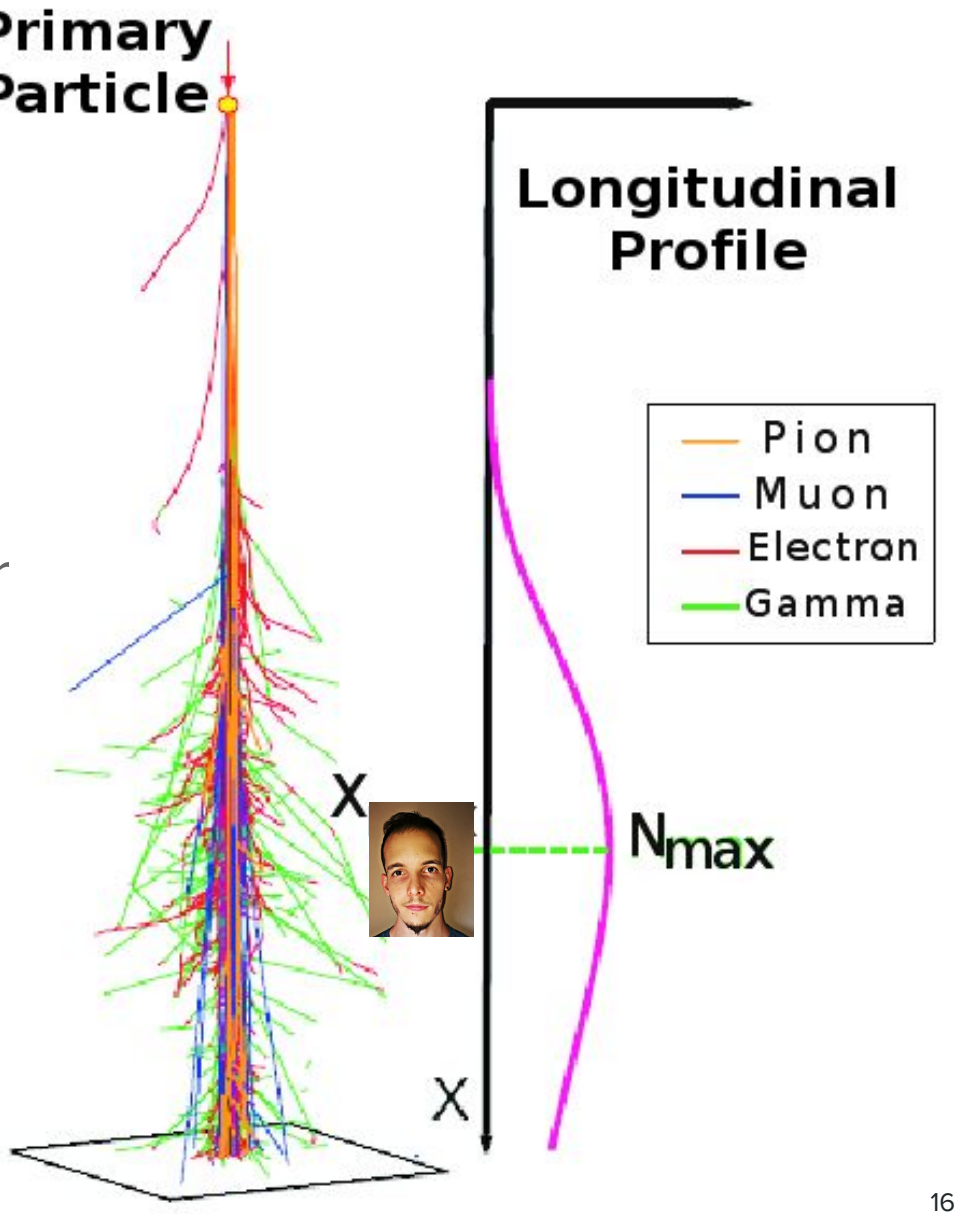

What do we measure?

Slant Depth

$$X(z) = \int_z^{\infty} \rho(\mathbf{r}(z'))dz'$$

→ **Amount of material traversed** by the shower at a z position on the shower axis.

$$X(z_{sea-level}) \sim 1000 \frac{g}{cm^2}$$

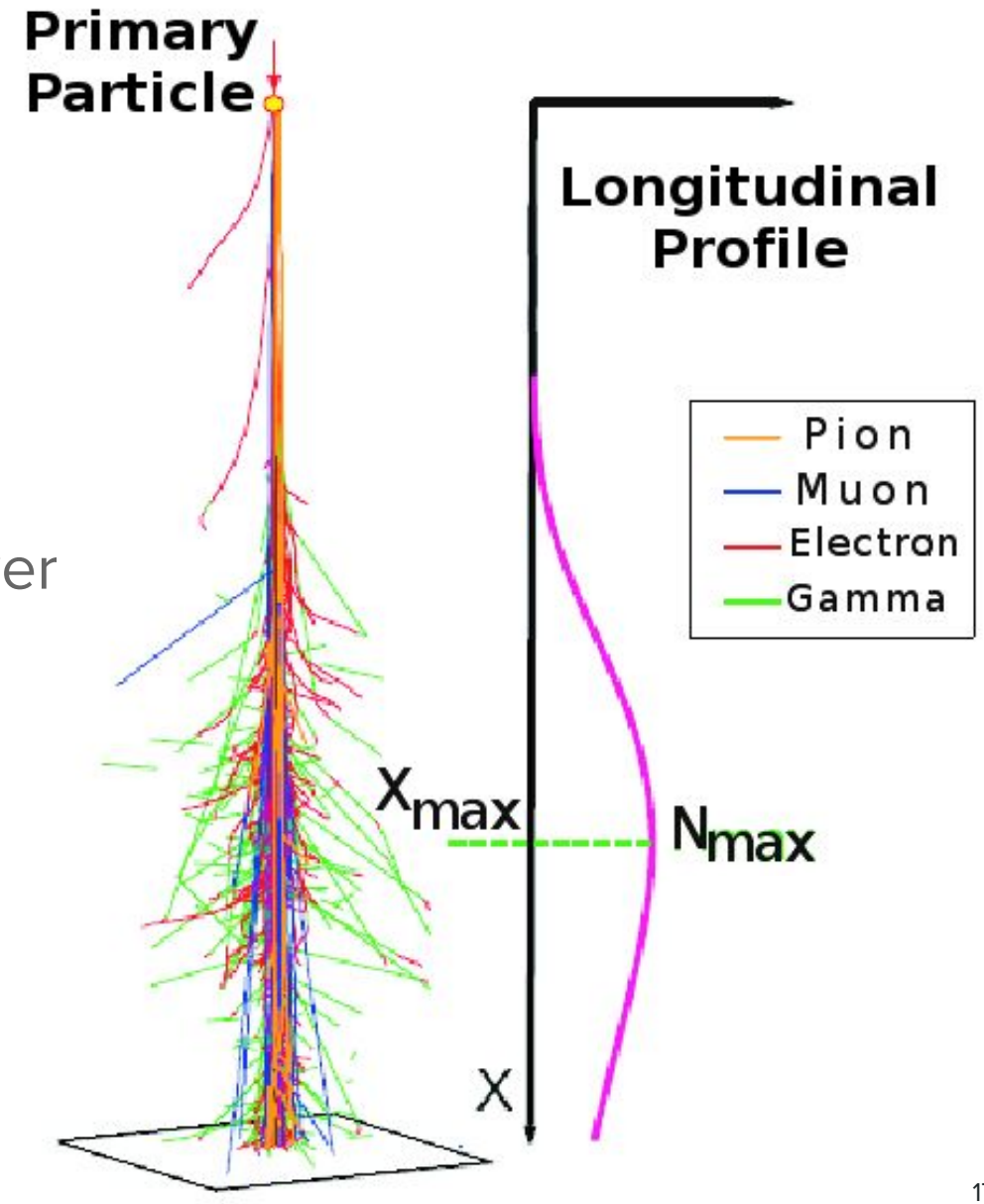

Reconstructing the air showers

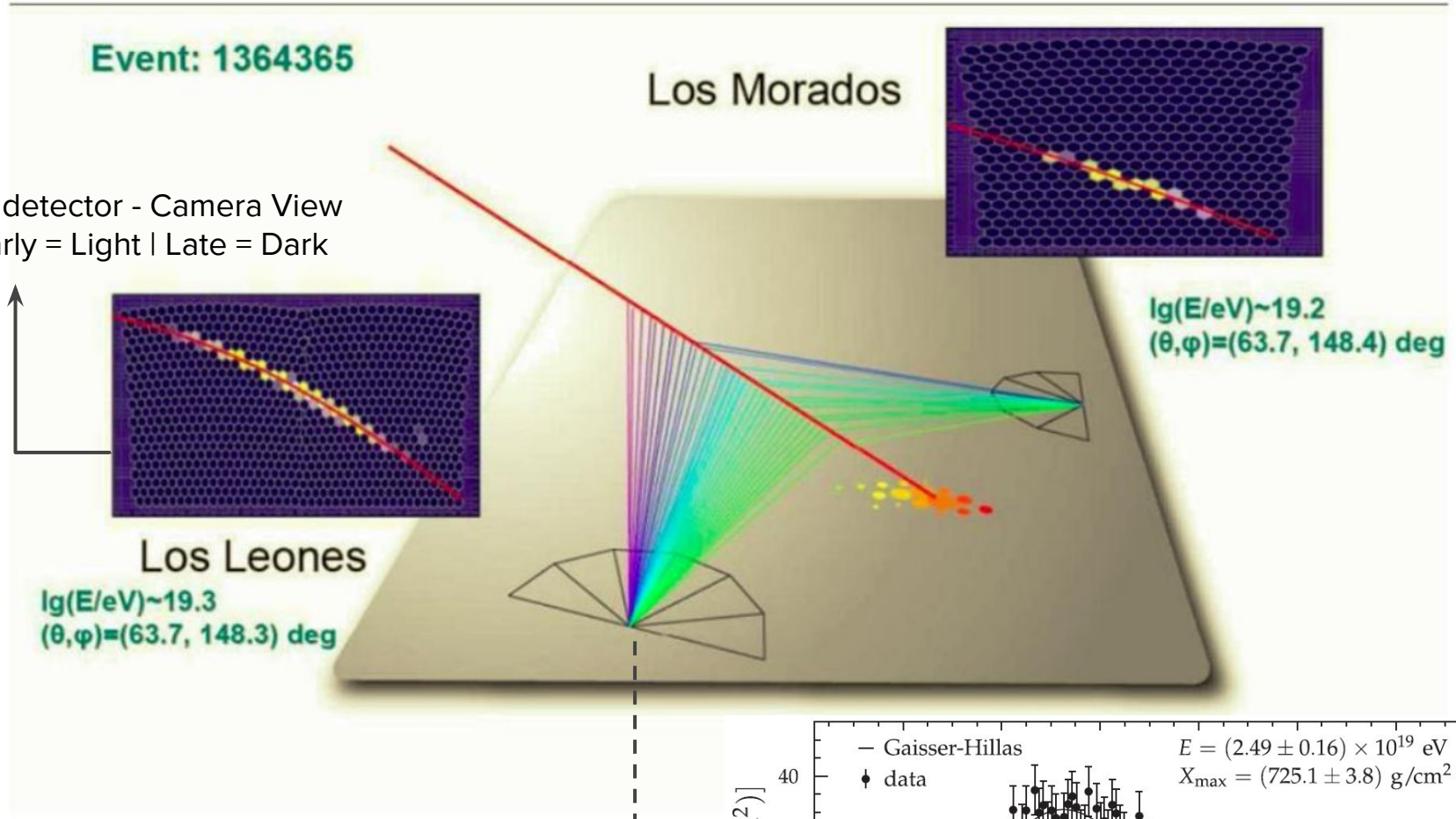

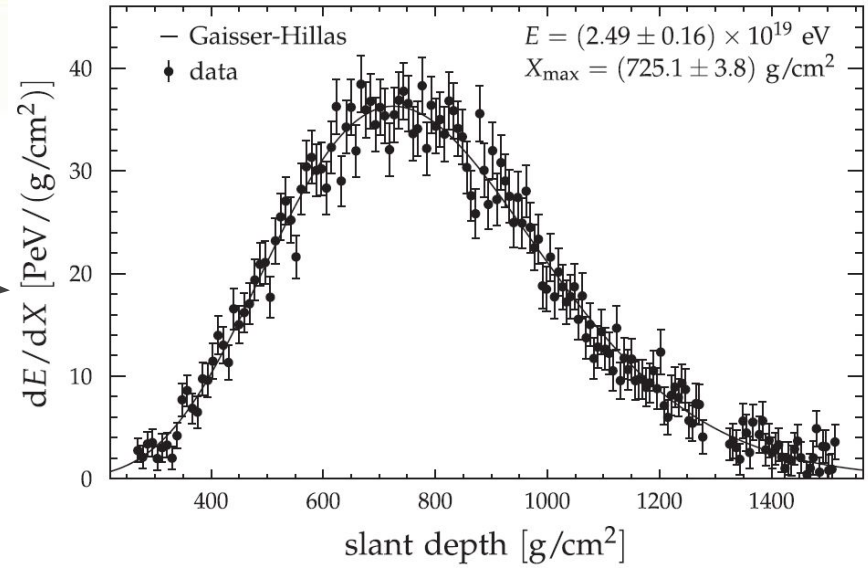

- **Energy** deposited is proportional to **number of particles**
- Fit profile to **obtain X_{max}**

Data Selection

Data Cut Flow

TABLE I. Event selection criteria, number of events after each cut and selection efficiency with respect to the previous cut.

Cut	Events	ε [%]
Pre-selection:		
Air-shower candidates	2573713	...
Hardware status	1920584	74.6
Aerosols	1569645	81.7
Hybrid geometry	564324	35.9
Profile reconstruction	539960	95.6
Clouds	432312	80.1
$E > 10^{17.8}$ eV	111194	25.7
Quality and fiducial selection:		
P(hybrid)	105749	95.1
X_{max} observed	73361	69.4
Quality cuts	58305	79.5
Fiducial field of view	21125	36.2
Profile cuts	19947	94.4

Data **Quality**

Optimal **Resolution** & Uniform **Acceptance**

Data collected from **December 1st 2004** to **December 31st 2012**

Pre-selection:		
Air-shower candidates	2573713	...
Hardware status	1920584	74.6
Aerosols	1569645	81.7
Hybrid geometry	564324	35.9
Profile reconstruction	539960	95.6
Clouds	432312	80.1
$E > 10^{17.8}$ eV	111194	25.7

Initial air-shower candidates

Data from one telescope with **misaligned optics** are not used

Require known **aerosol** conditions

Pre-selection:		
Air-shower candidates	2573713	...
Hardware status	1920584	74.6
Aerosols	1569645	81.7
Hybrid geometry	564324	35.9
Profile reconstruction	539960	95.6
Clouds	432312	80.1
$E > 10^{17.8}$ eV	111194	25.7

Initial air-shower candidates

Data from one telescope with **misaligned optics** are not used

Require known **aerosol** conditions

Pre-selection:		
Air-shower candidates	2573713	...
Hardware status	1920584	74.6
Aerosols	1569645	81.7
Hybrid geometry	564324	35.9
Profile reconstruction	539960	95.6
Clouds	432312	80.1
$E > 10^{17.8}$ eV	111194	25.7

Initial air-shower candidates

Data from one telescope with **misaligned optics** are not used

Require known **aerosol** conditions

Pre-selection:		
Air-shower candidates	2573713	...
Hardware status	1920584	74.6
Aerosols	1569645	81.7
Hybrid geometry	564324	35.9
Profile reconstruction	539960	95.6
Clouds	432312	80.1
$E > 10^{17.8}$ eV	111194	25.7

Full **shower reconstruction** is required

Full longitudinal **profile reconstruction**

Lower **energy threshold** for the analysis

Possible reflection or shadowing by **clouds**

Quality and fiducial selection:		
P(hybrid)	105749	95.1
X_{max} observed	73361	69.4
Quality cuts	58305	79.5
Fiducial field of view	21125	36.2
Profile cuts	19947	94.4

Avoid bias in triggering of heavy nucleus vs. proton showers

Select showers **containing X_{max}**

Quality and fiducial selection:		
P(hybrid)	105749	95.1
X_{max} observed	73361	69.4
Quality cuts	58305	79.5
Fiducial field of view	21125	36.2
Profile cuts	19947	94.4

Avoid bias in triggering of heavy nucleus vs. proton showers

Select showers **containing X_{max}**

Quality and fiducial selection:		
P(hybrid)	105749	95.1
X_{max} observed	73361	69.4
Quality cuts	58305	79.5
Fiducial field of view	21125	36.2
Profile cuts	19947	94.4

Veto **highly collimated** and **faint** showers

Select only **"good" showers**

“Good” quality shower

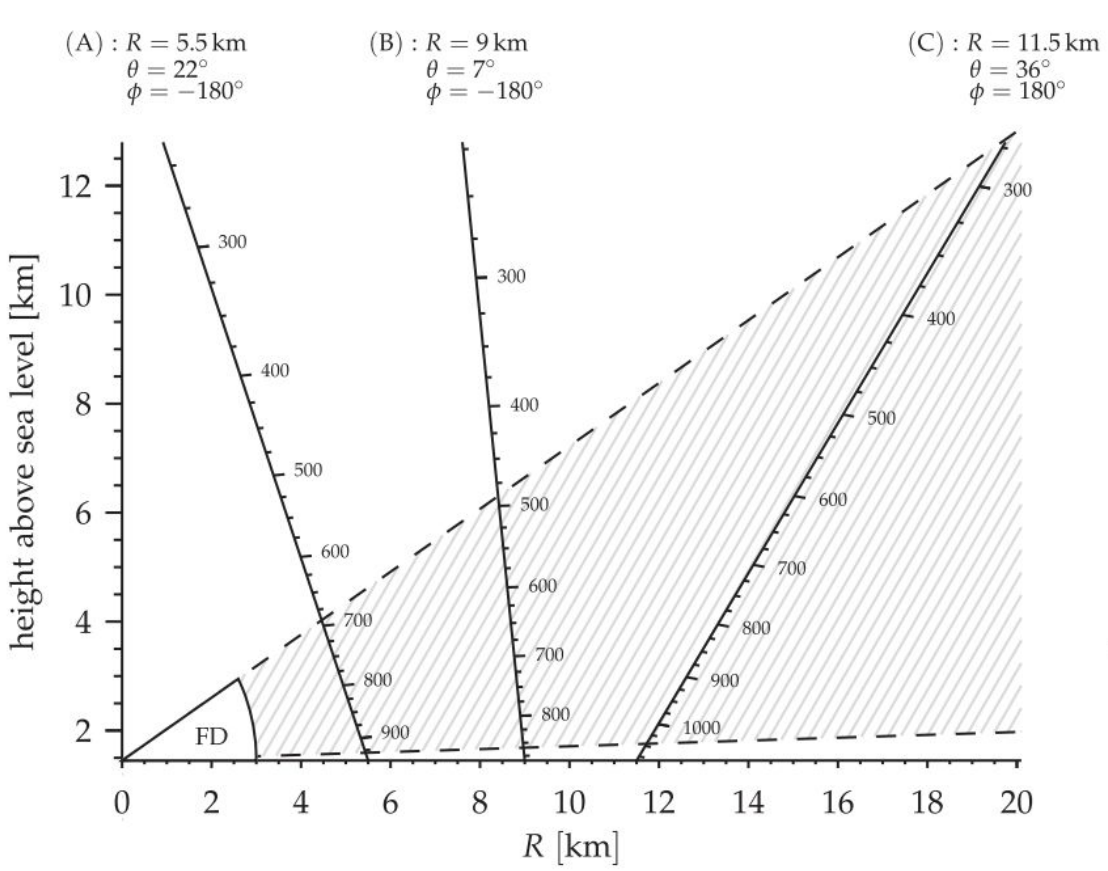

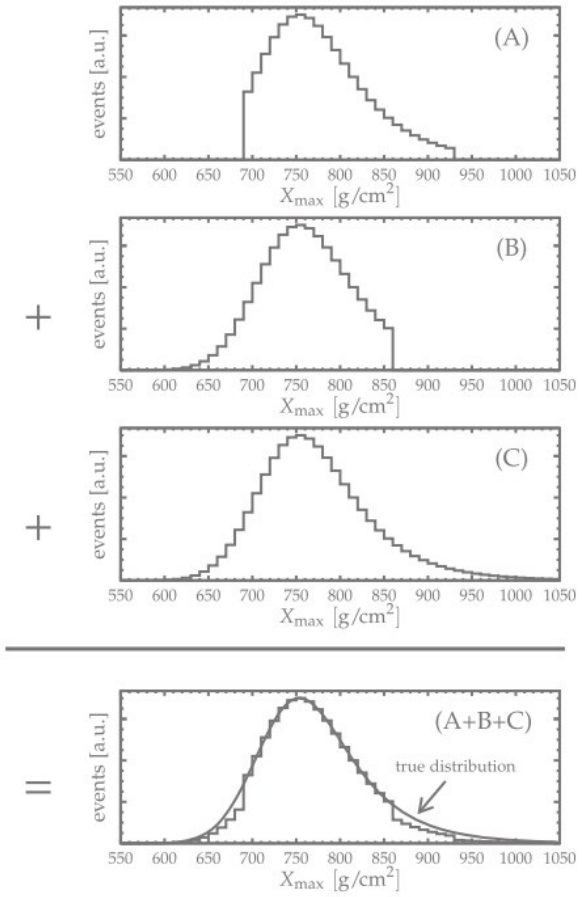

“Good” quality shower

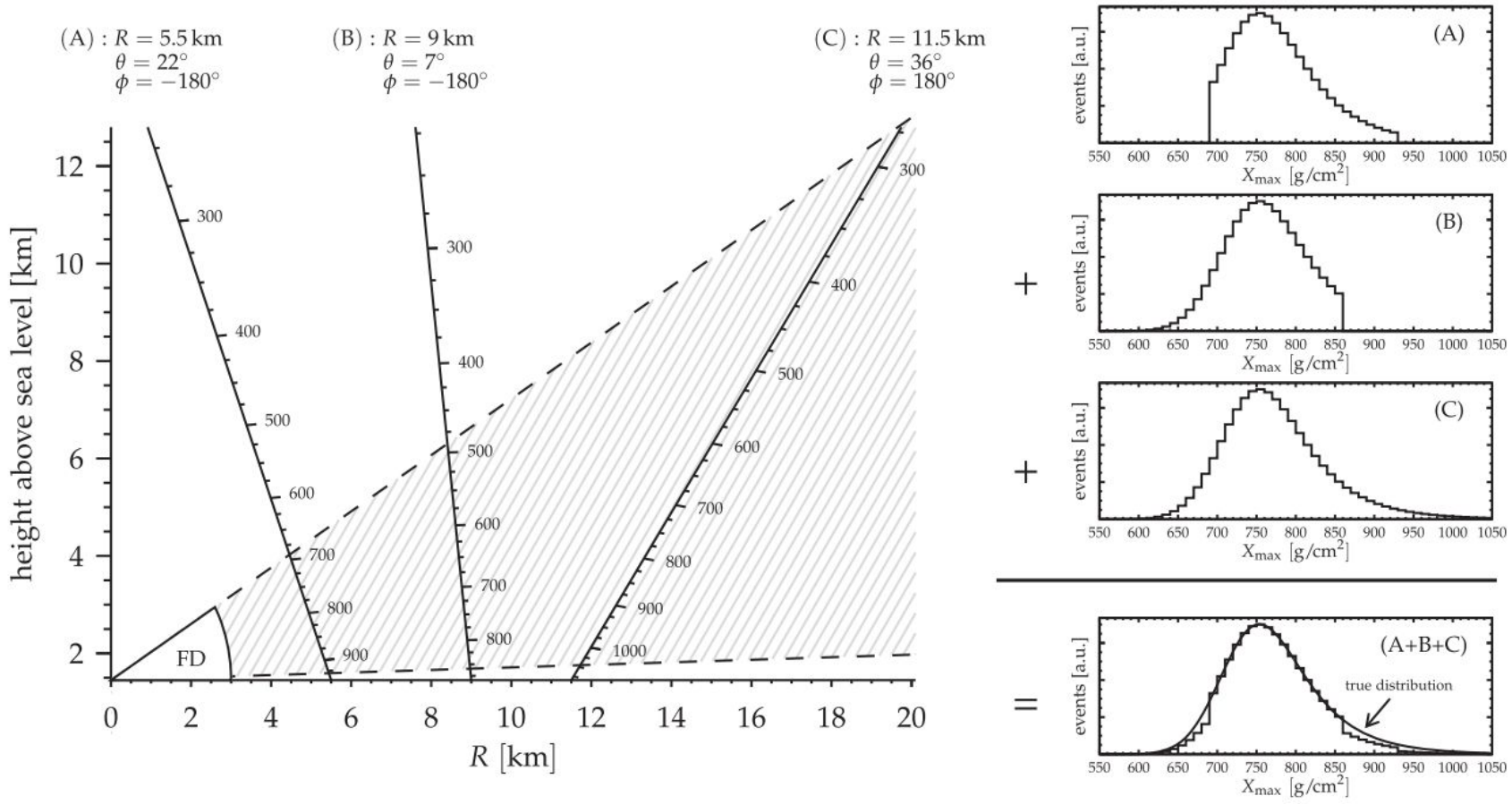

“Good” quality shower

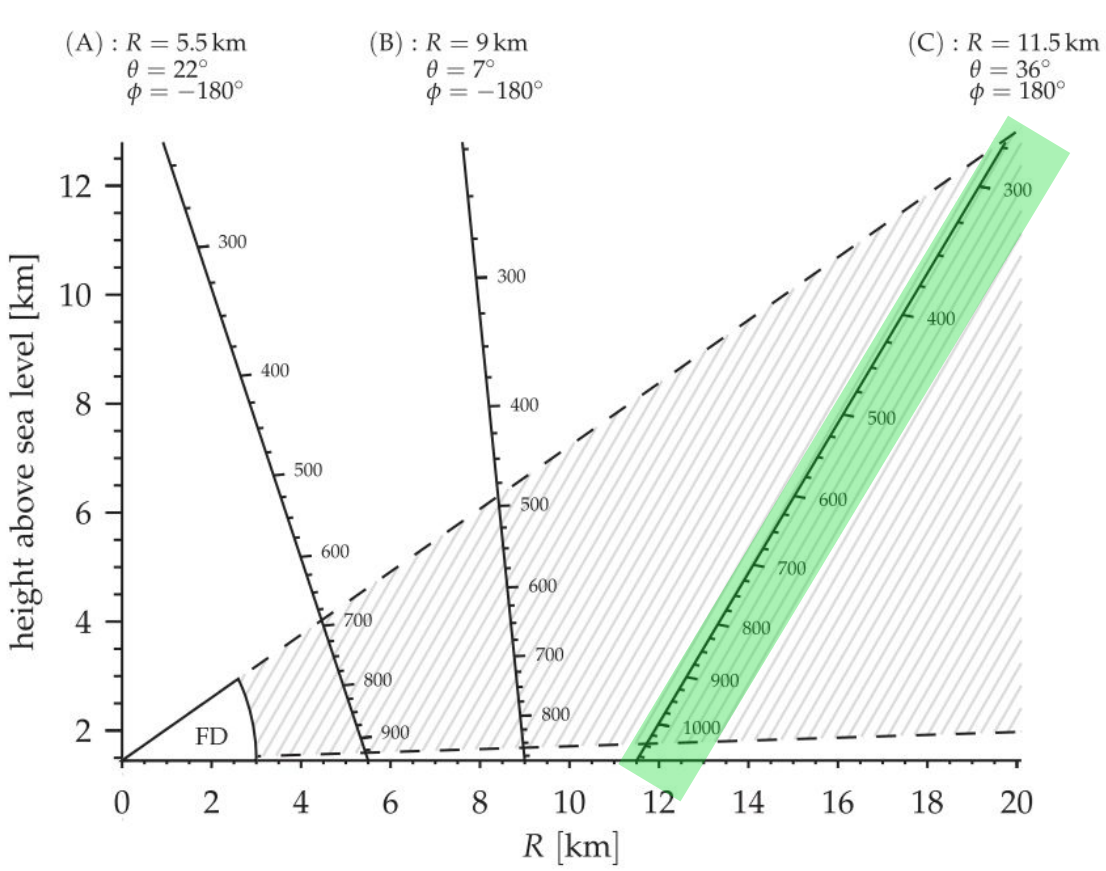

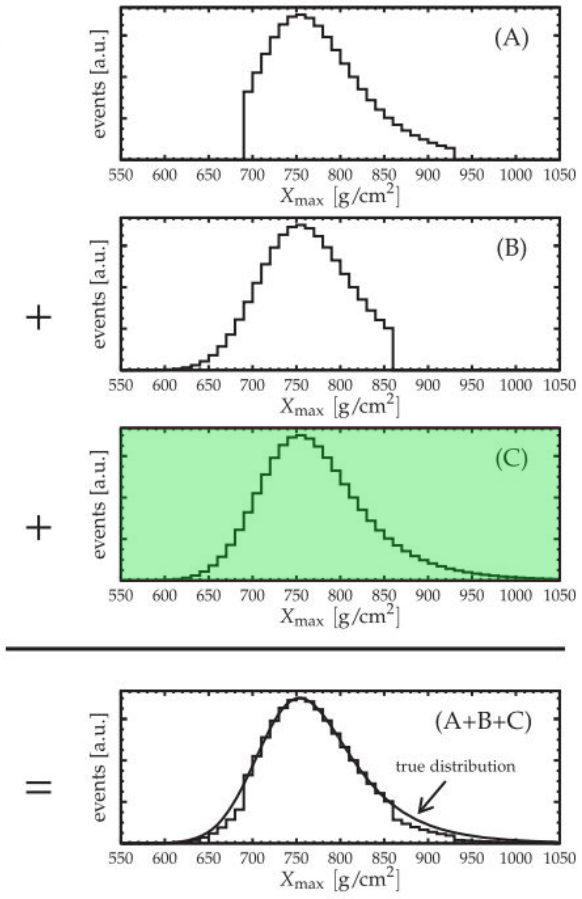

“Good” quality shower

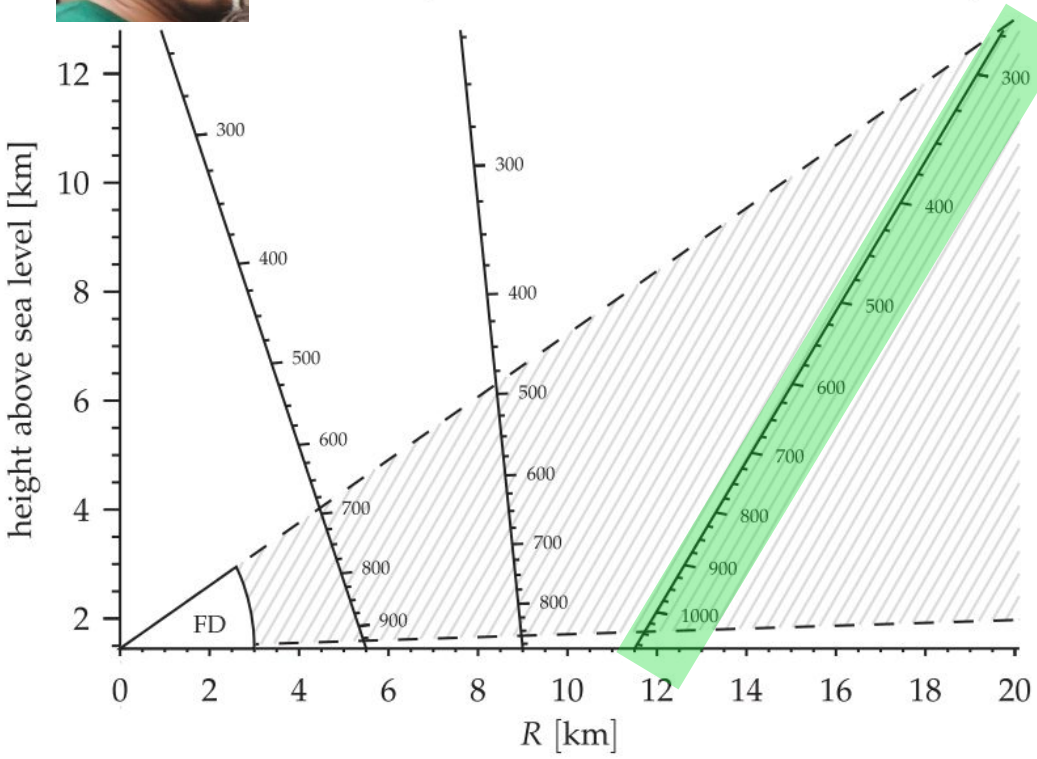

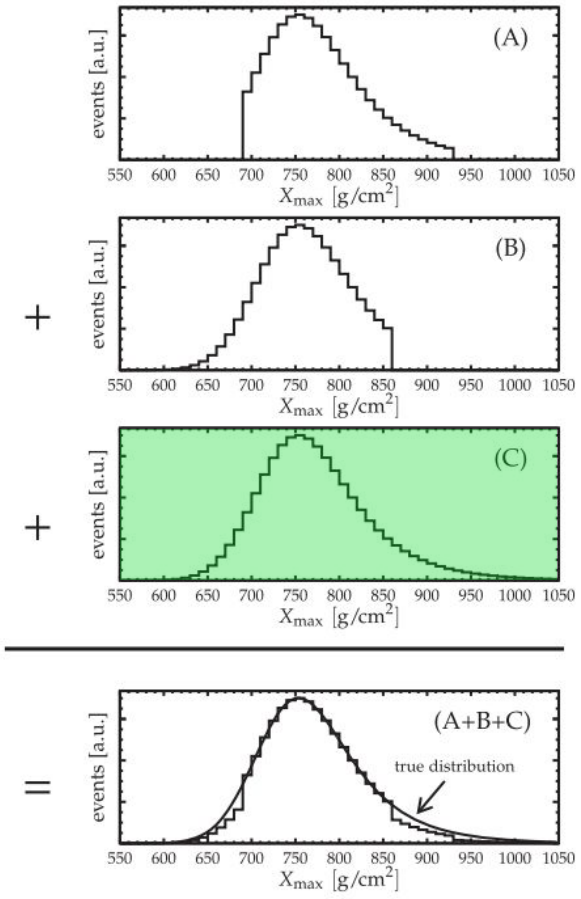

“Good” quality shower

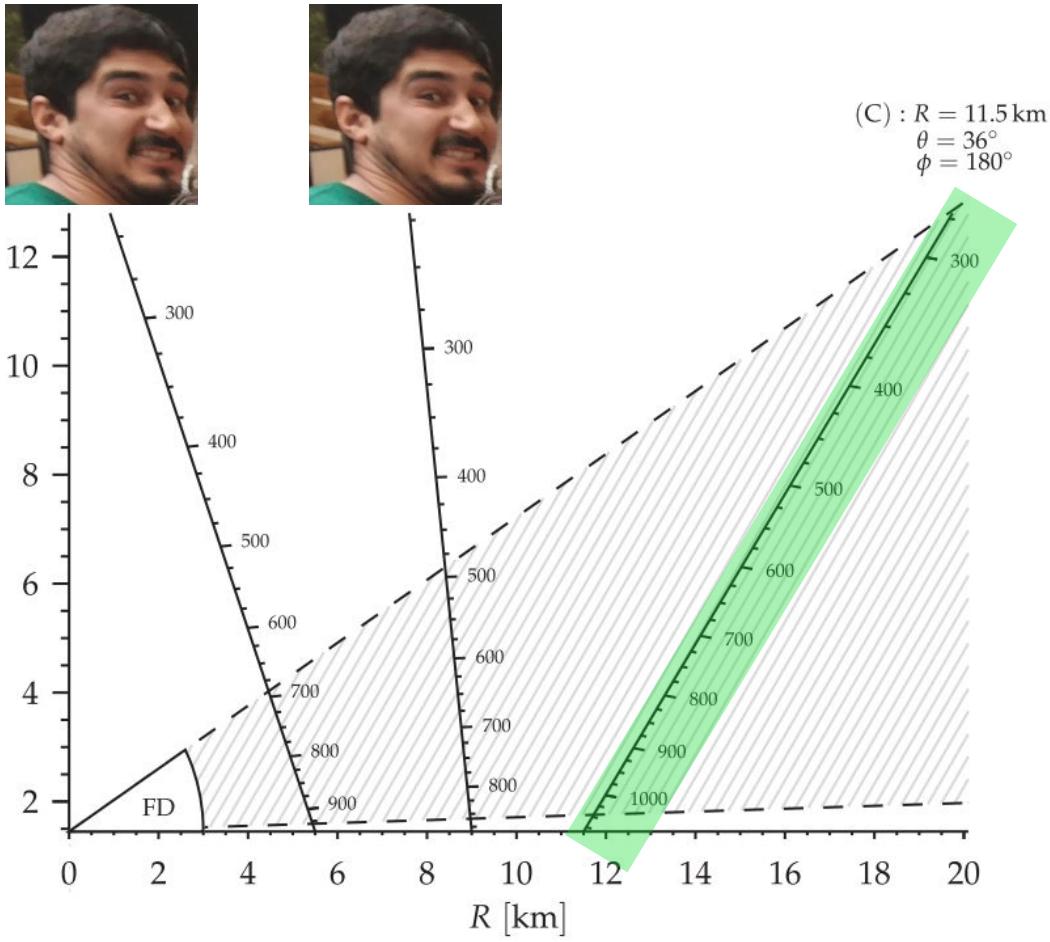

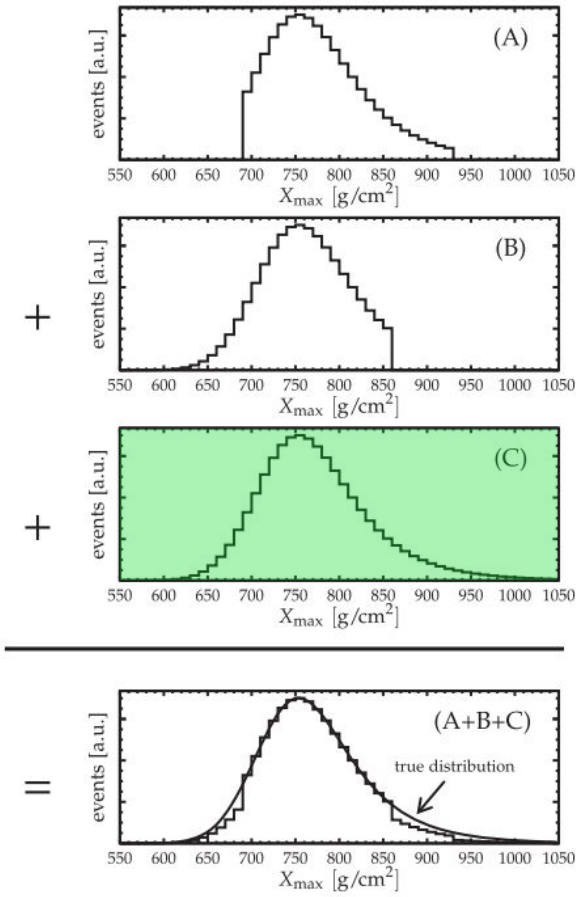

“Good” quality shower

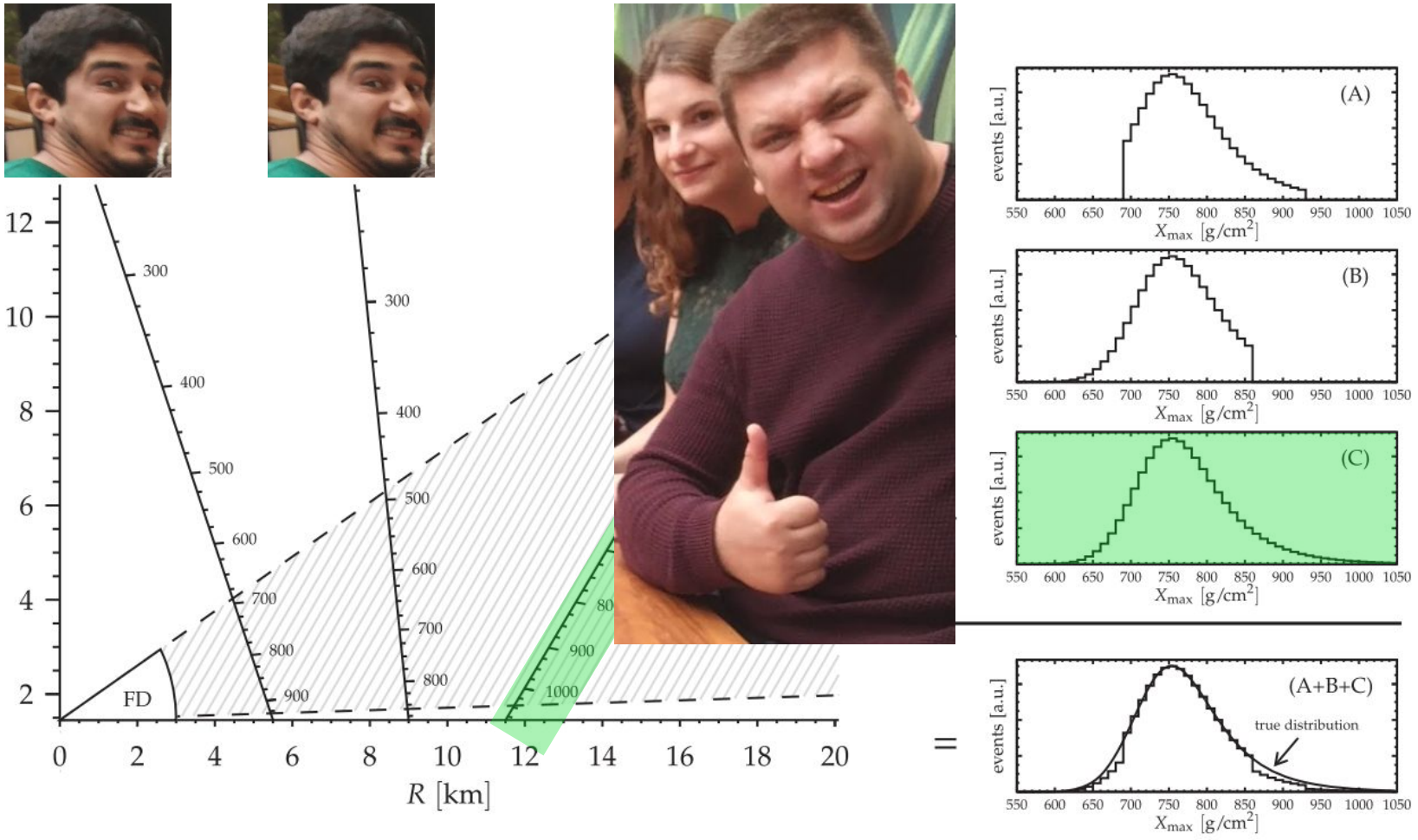

Avoid bias in triggering of heavy nucleus vs. proton showers

Select showers **containing X_{max}**

Quality and fiducial selection:		
P(hybrid)	105749	95.1
X_{max} observed	73361	69.4
Quality cuts	58305	79.5
Fiducial field of view	21125	36.2
Profile cuts	19947	94.4

Veto **highly collimated** and **faint** showers

Select only **"good" showers**

Avoid bias in triggering of heavy nucleus vs. proton showers

Select showers **containing X_{max}**

Quality and fiducial selection:		
P(hybrid)	105749	95.1
X_{max} observed	73361	69.4
Quality cuts	58305	79.5
Fiducial field of view	21125	36.2
Profile cuts	19947	94.4

Reject events with **uninstrumented gaps**, residual **cloud** and **dust**, etc.

Select only **"good" showers**

Veto **highly collimated** and **faint** showers

Resolution

Resolution determines the width of the distribution of X^{rec}_{max} around the true X_{max}

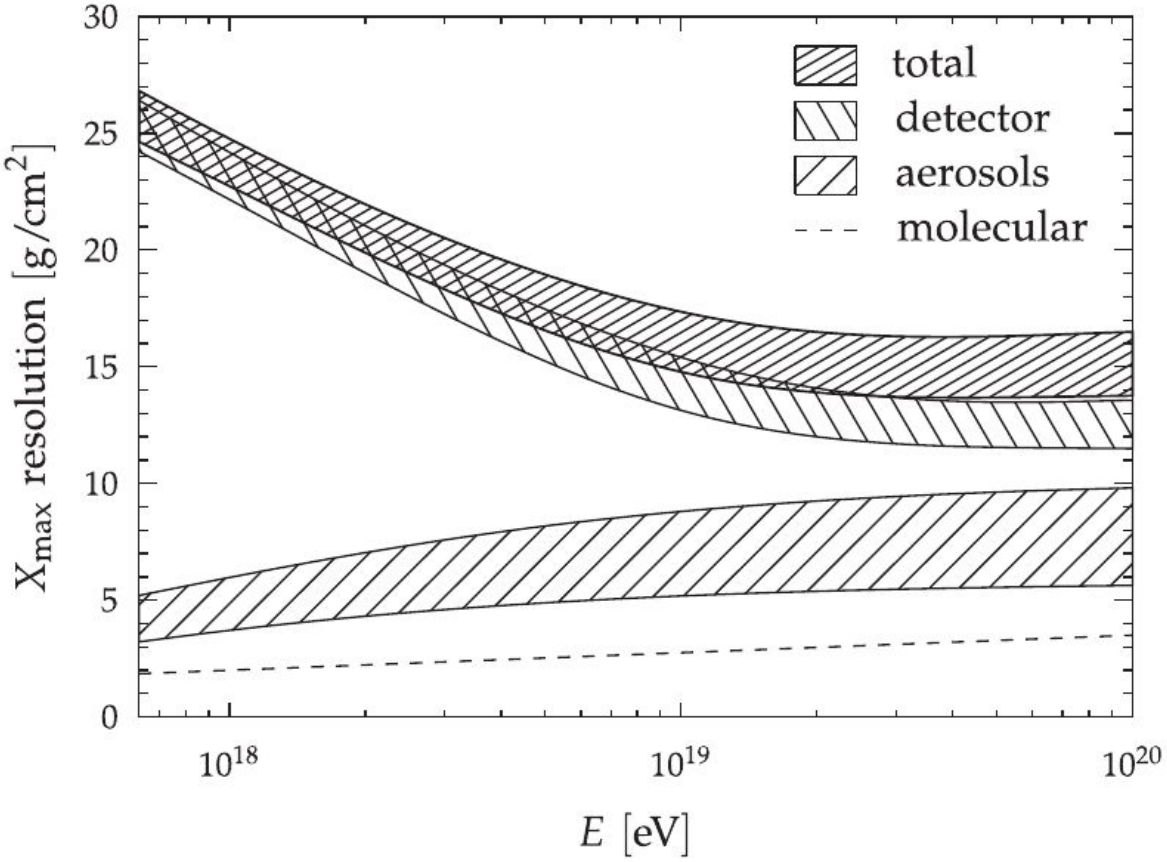

Detector

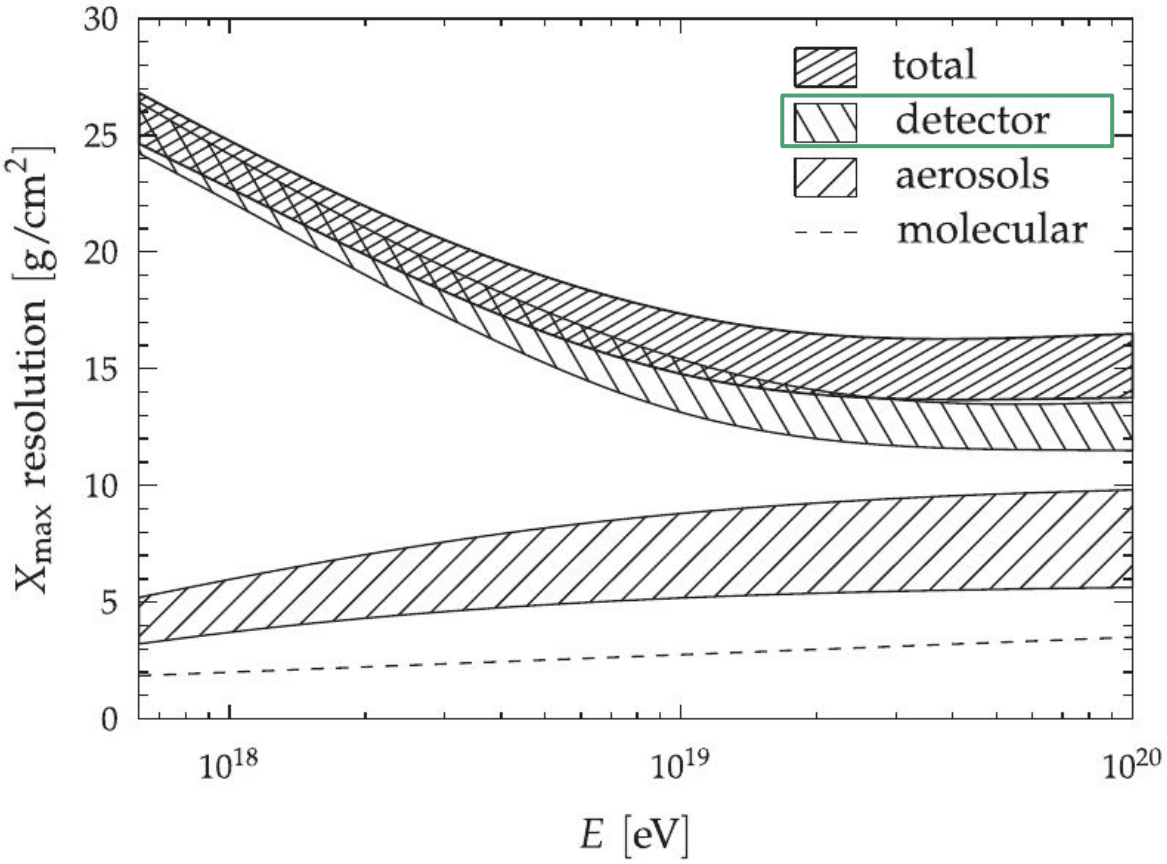

- **Stat. fluctuations** of the number of photoelectrons detected
- Reconstruction of the **arrival direction**
- **Energy-dependant** resolution
- **Alignment** of telescopes

Aerosols

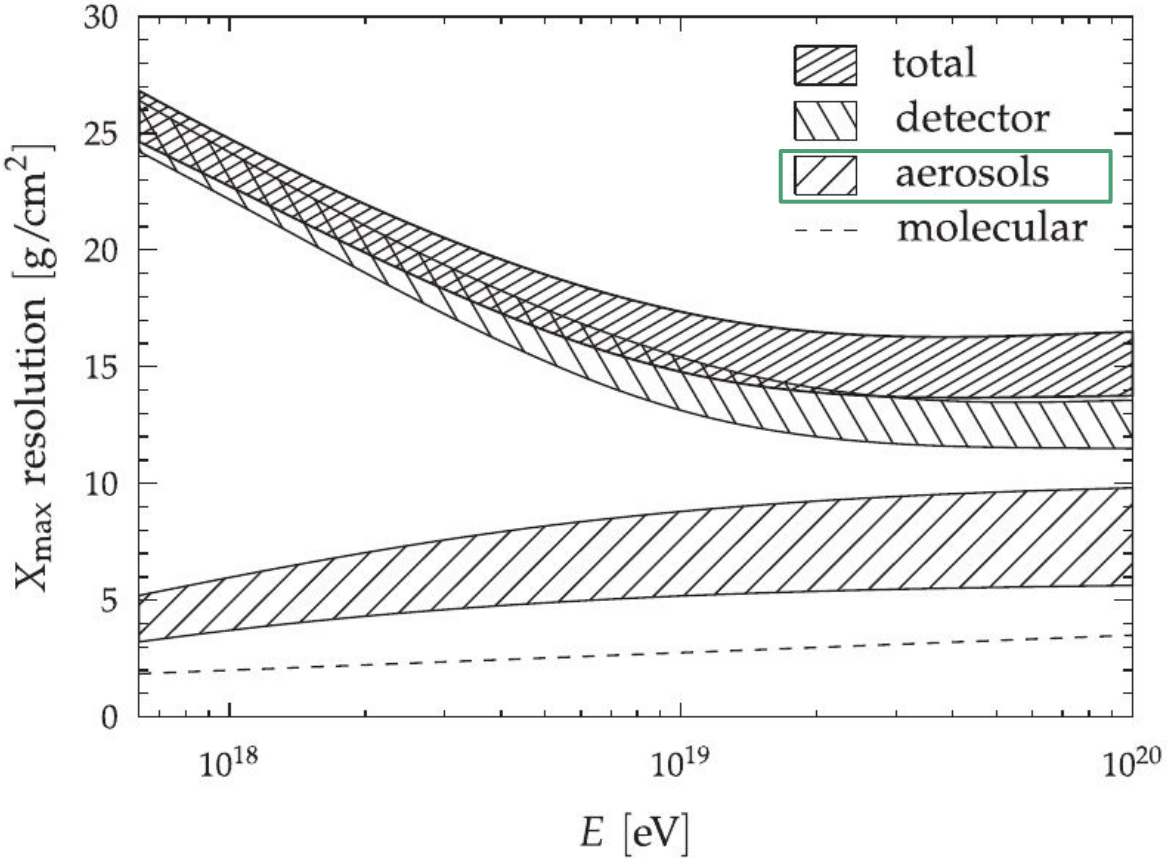

- Fluctuations of the **night sky background**
- Time variability of the aerosol content
- **Non-uniformity** of the **aerosol layers** across the array

Molecular atmosphere

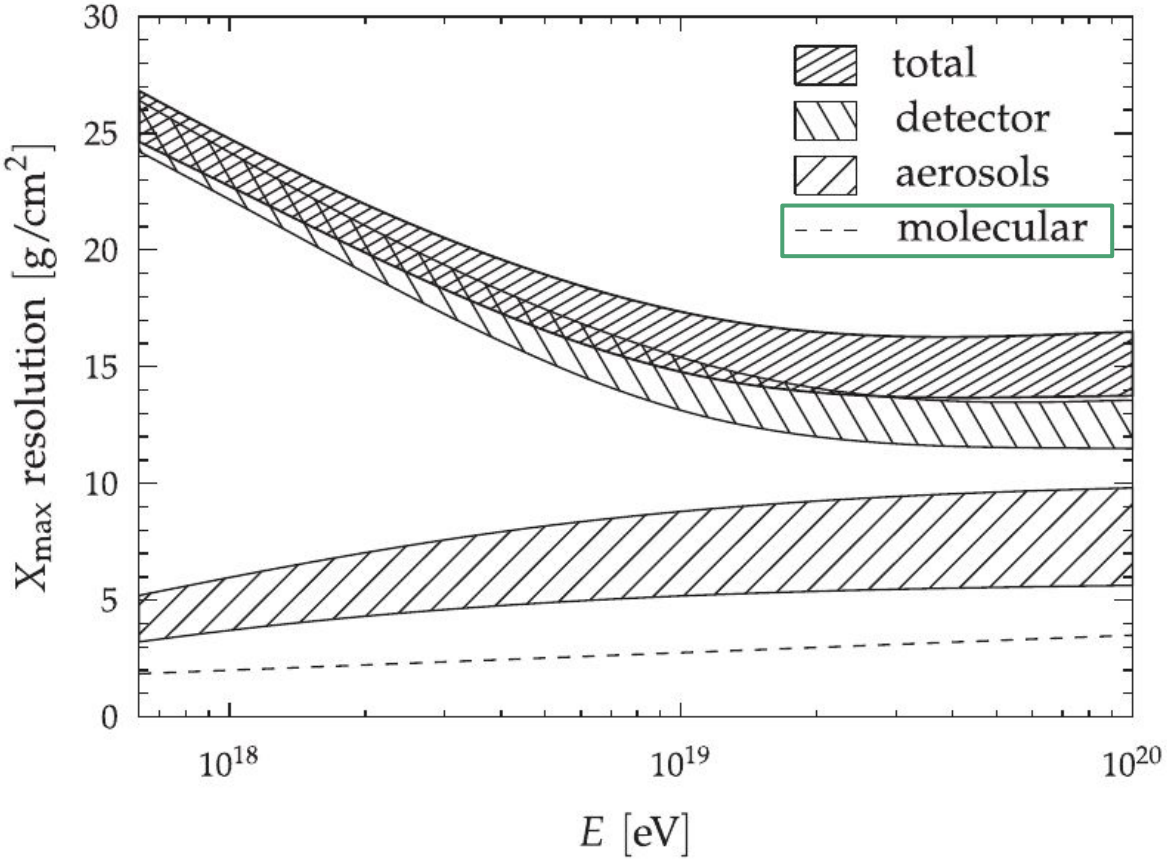

- Precision of the **density profile of the atmosphere**

Syste“Matt”ic Uncertainties

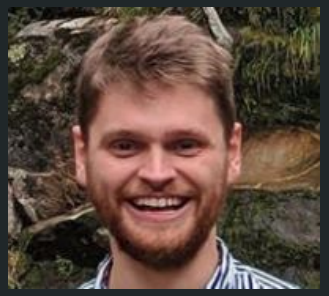

Syste“Matt”ic Uncertainties

Syste“Matt”ic Uncertainties

Systematics

- **Reconstruction** systematics dominant at low energies
- **Atmospheric** systematics dominant at high energies

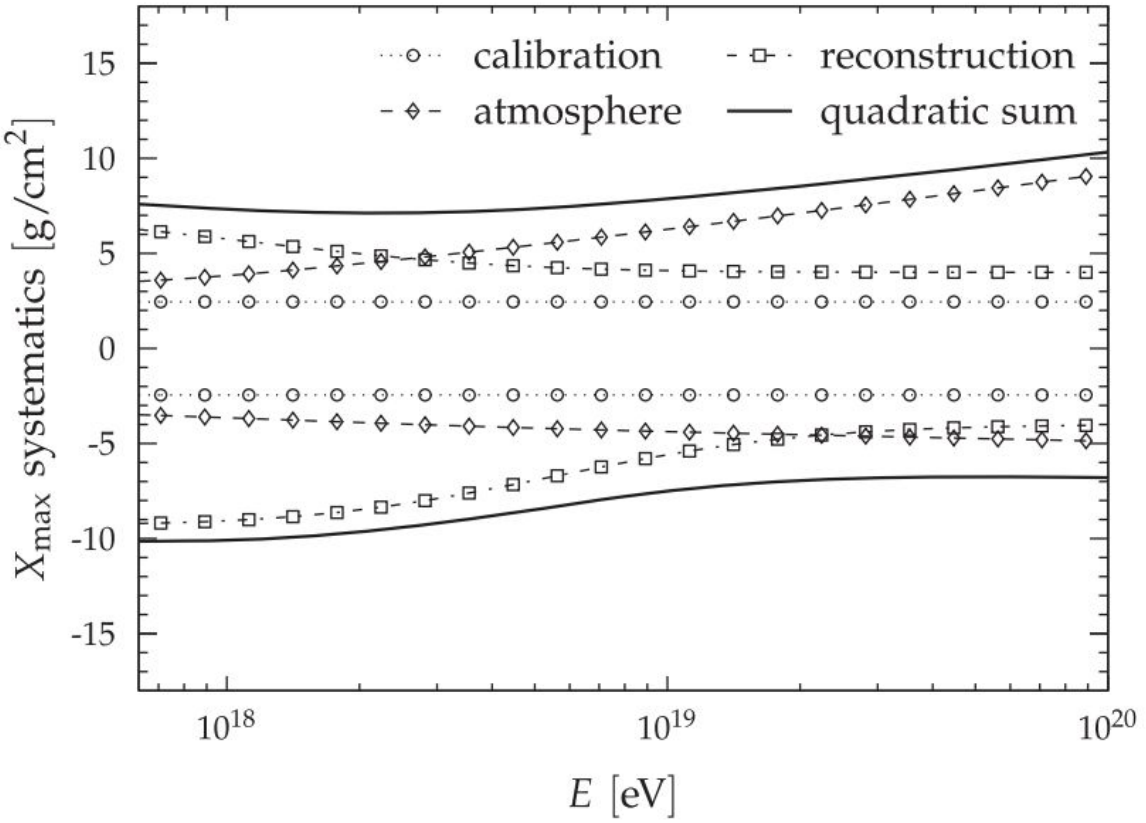

Systematics: Reconstruction

- **Reconstruction** uncertainty:
  - Longitudinal and lateral **shower shape** mismodeleing

↳ Estimated comparing **data to simulations**

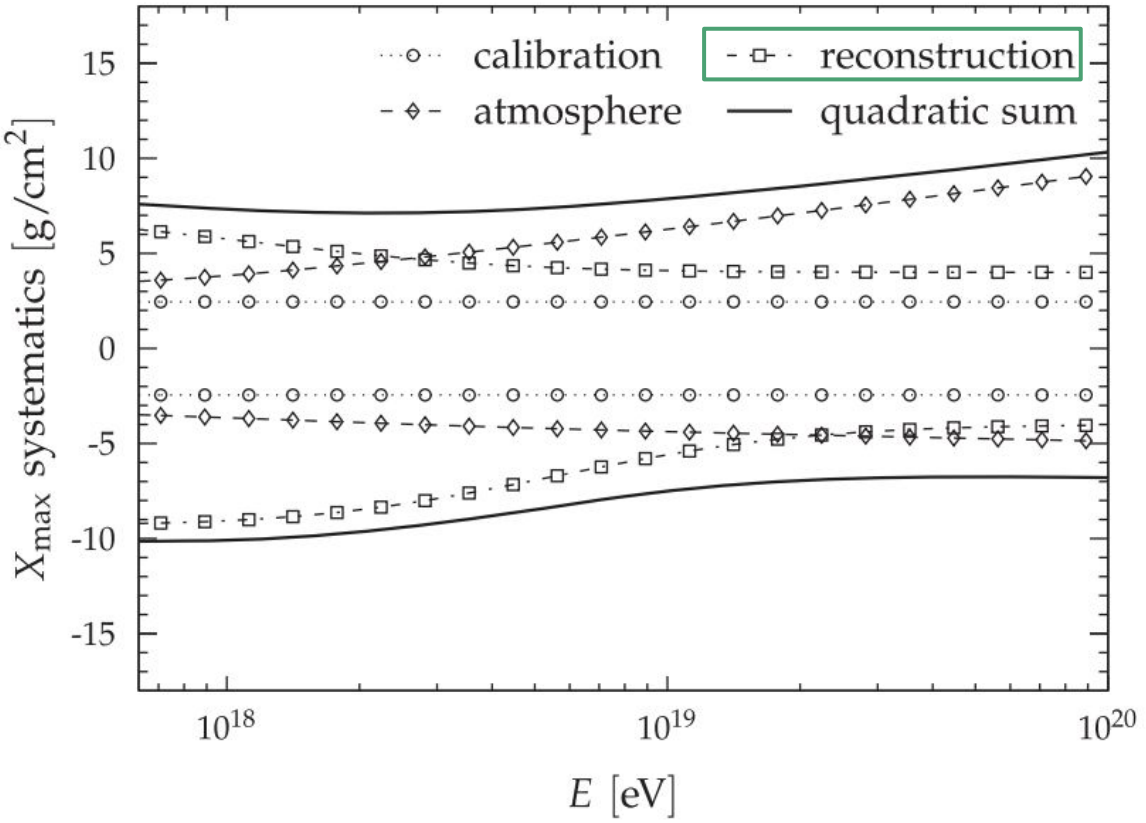

Systematics: Atmosphere

- **Atmospheric** uncertainty:
  - Non-uniformity of aerosol **concentration**
  - **Yield** of fluorescent light

↳ Estimated from **atmospheric monitoring studies**

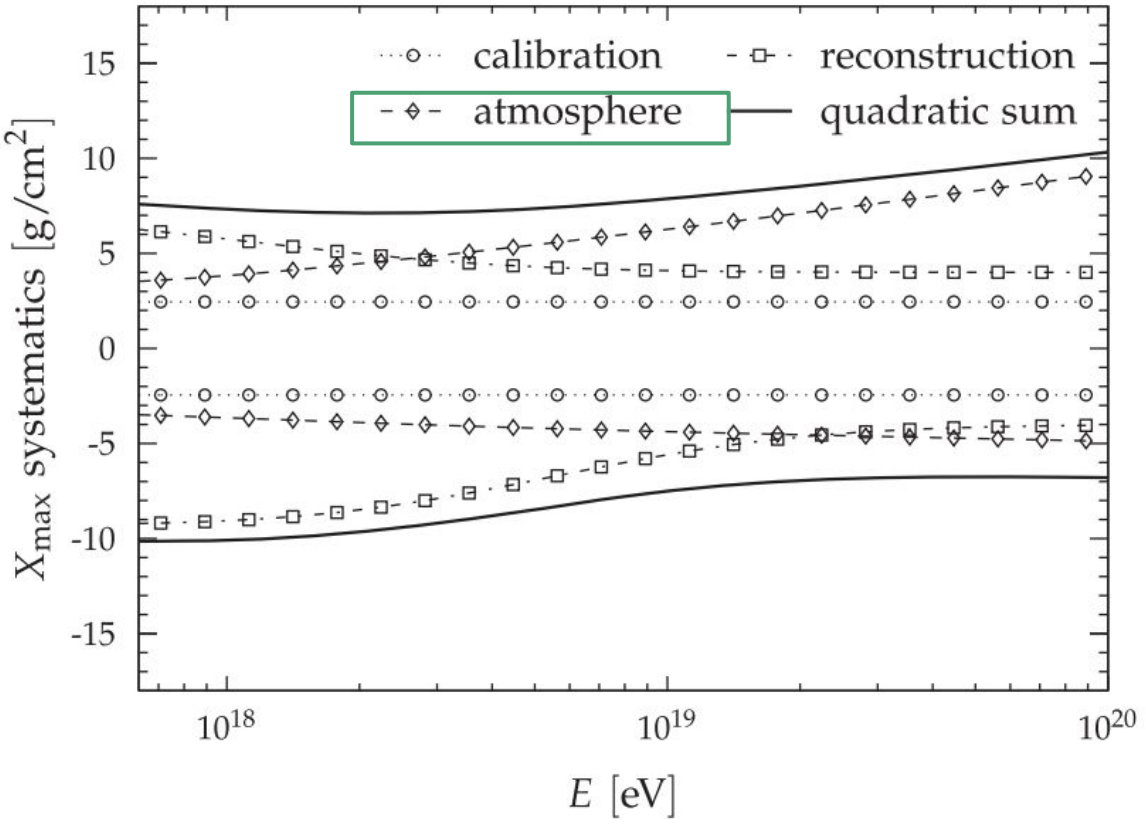

Systematics: Detector Calibration

- **Detector Calibration:**
  - Relative **timing** between **FD** and **SD**
  - **Alignment**
  - **Gains** in photomultipliers

↳ Estimated by **re-running reconstruction** with varied parameters

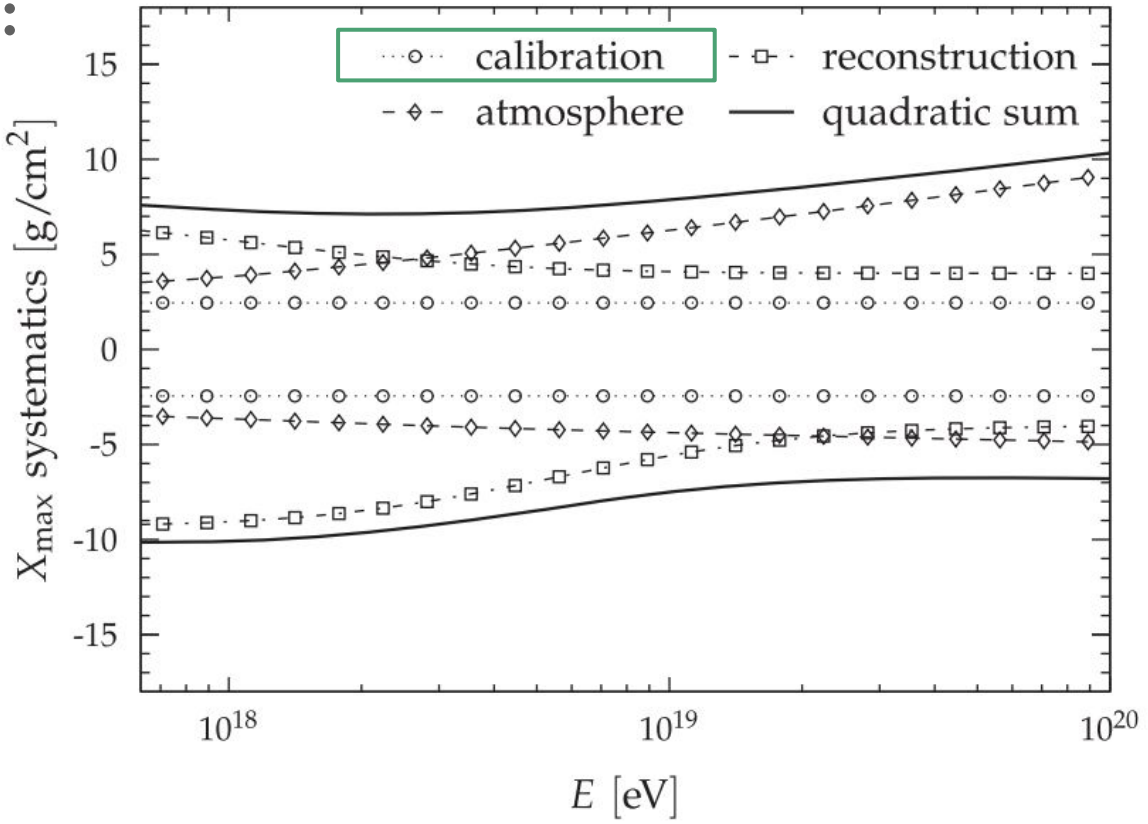

Results

X_{max} distributions

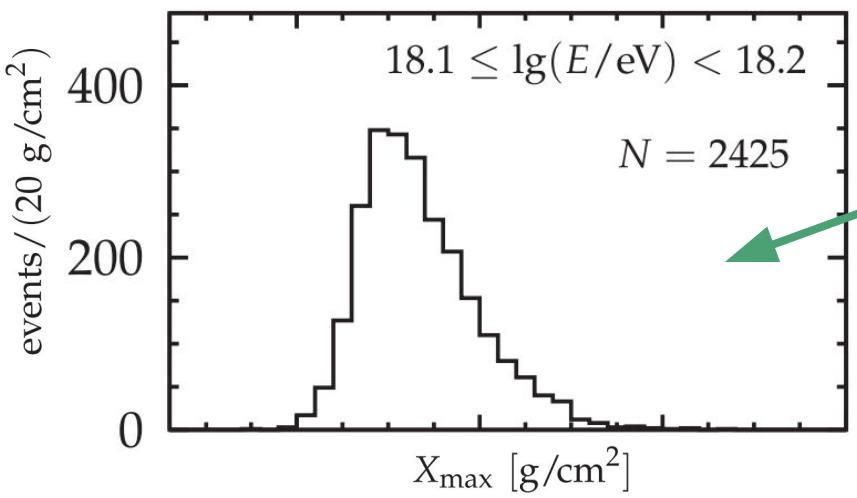

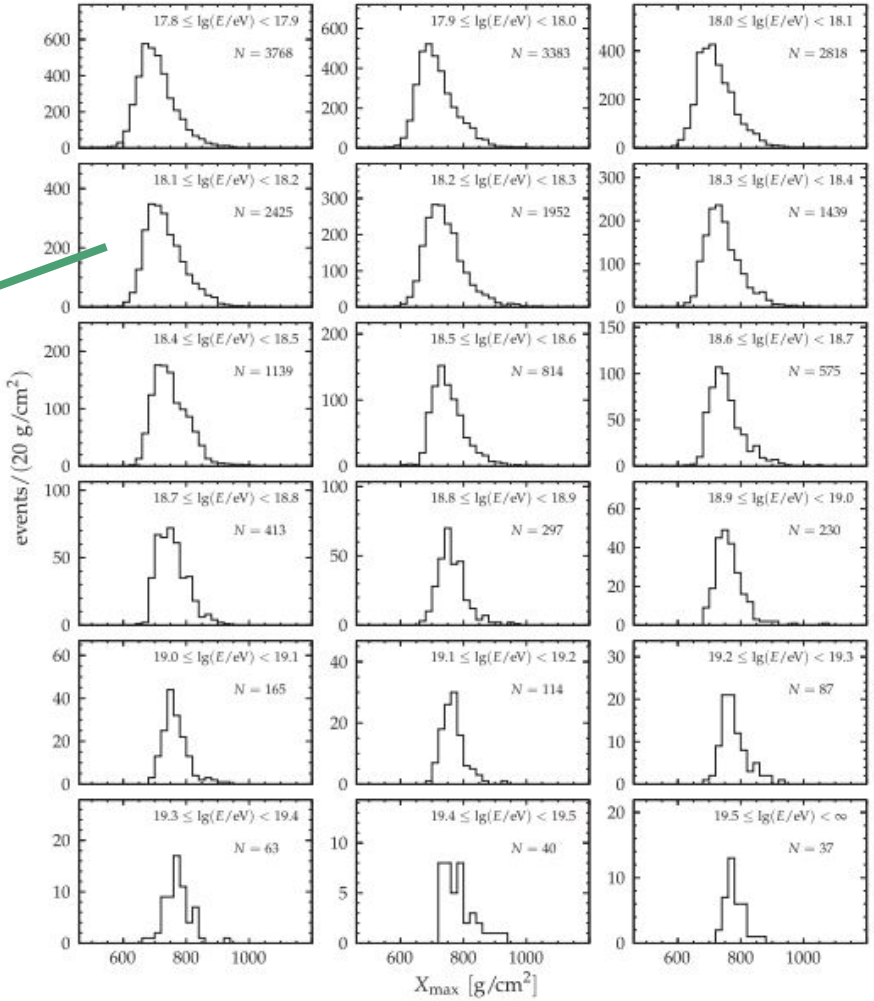

Bin convention:

- Energies from $10^{17.8}$ to $10^{19.5}$ eV bins of Δ lg (E/eV) = 0.1
- Energies above $10^{19.5}$ eV an integral bin is used

X_{max} and $\sigma(X_{max})$ as a function of shower energy

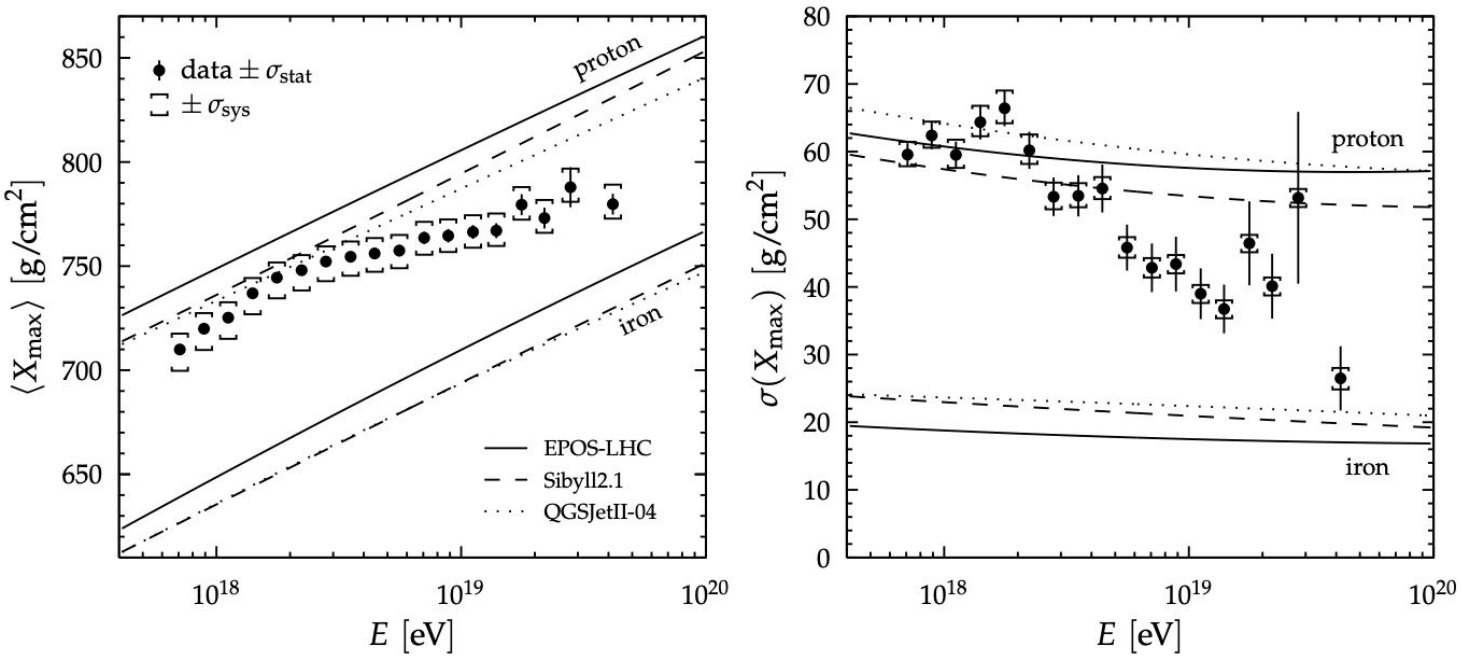

Fig. Energy evolution of the first two central moments of the X_{max} distribution compared to air-shower simulations for proton and iron primaries

X_{max} and $\sigma(X_{max})$ as a function of shower energy

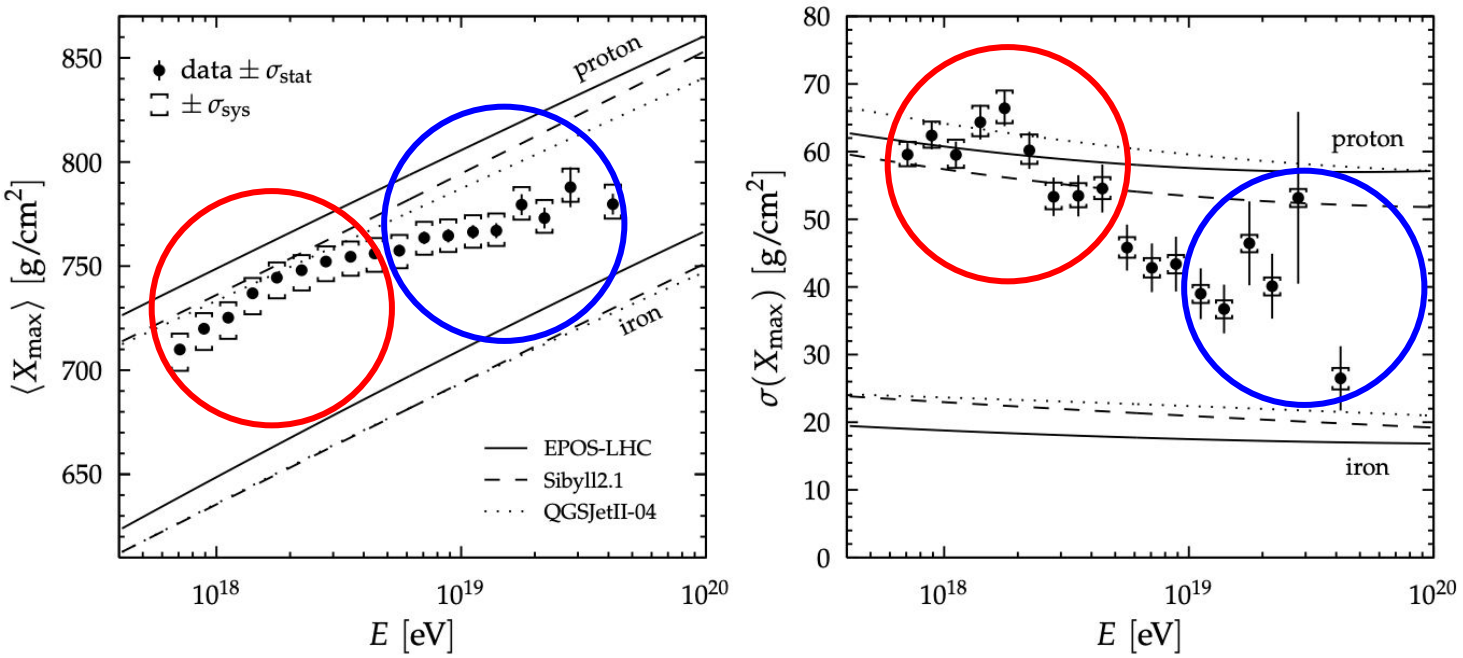

Fig. Energy evolution of the first two central moments of the X_{max} distribution compared to air-shower simulations for proton and iron primaries

High energy: tendency for **heavier** composition

Lower energy: tendency for **lighter** composition

Mass of primary interpretation

- Based in various **models of hadronic interactions**, we can obtain an

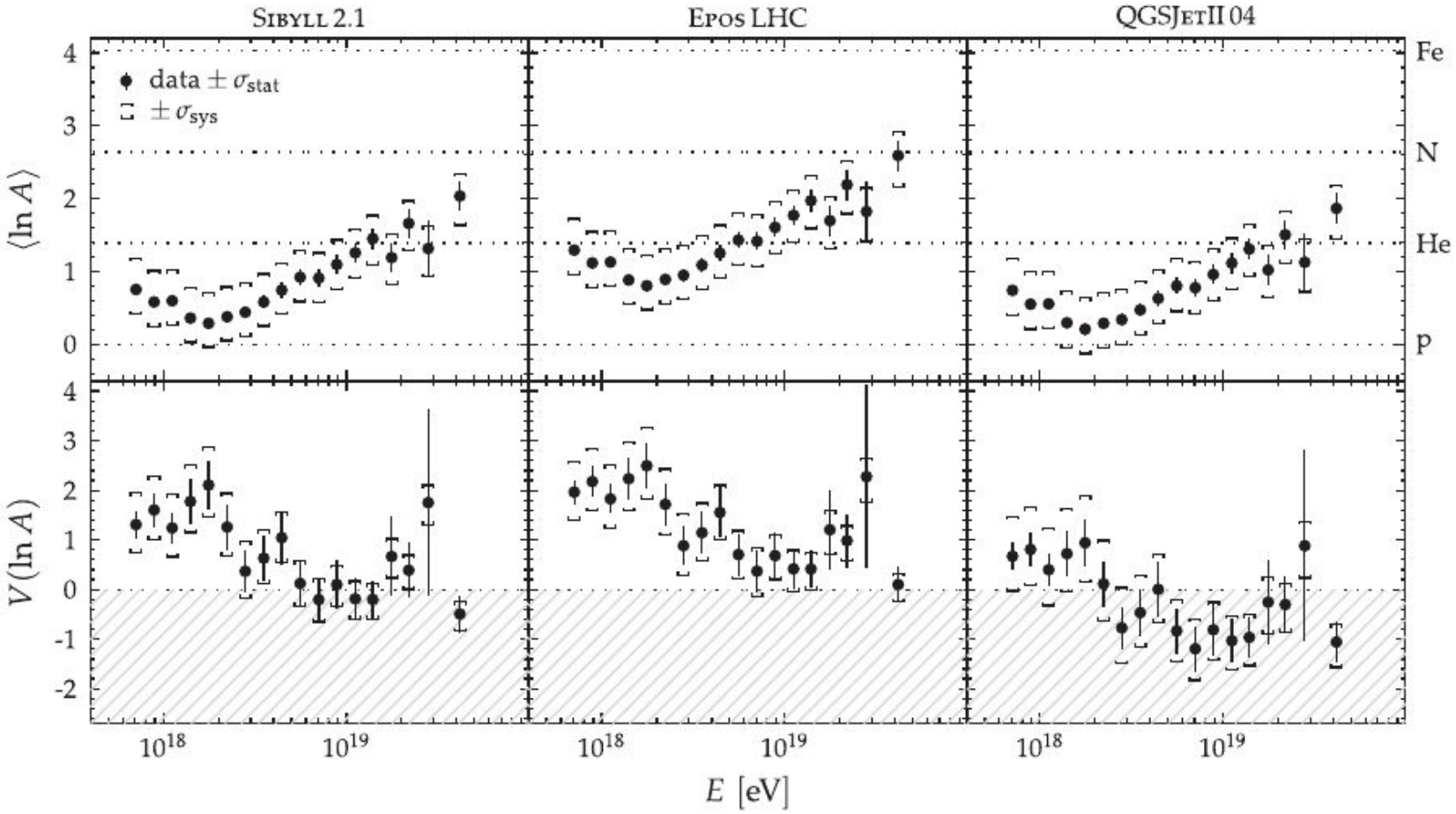

Average of the logarithmic mass (**<lnA>**) and its variance (**V(lnA)**)

Summary and Conclusions

- A **measurement** of the **shower depth maximum X_{max}** of high-energy cosmic rays was presented.
- **Largest** sample of X_{max} ever obtained by a cosmic-ray detector was collected.
- **All results** are **freely available** to be used in interpretations of the measurements, **facilitating comparison** to other experiments.
- An **interpretation** in terms of **mass composition** is performed, which suggests that cosmic-rays are composed of **light nuclei up to $10^{18.3}$ eV** and the fraction of **heavy nuclei** increases **up to** energies to **$10^{19.6}$ eV**.

Thank you!

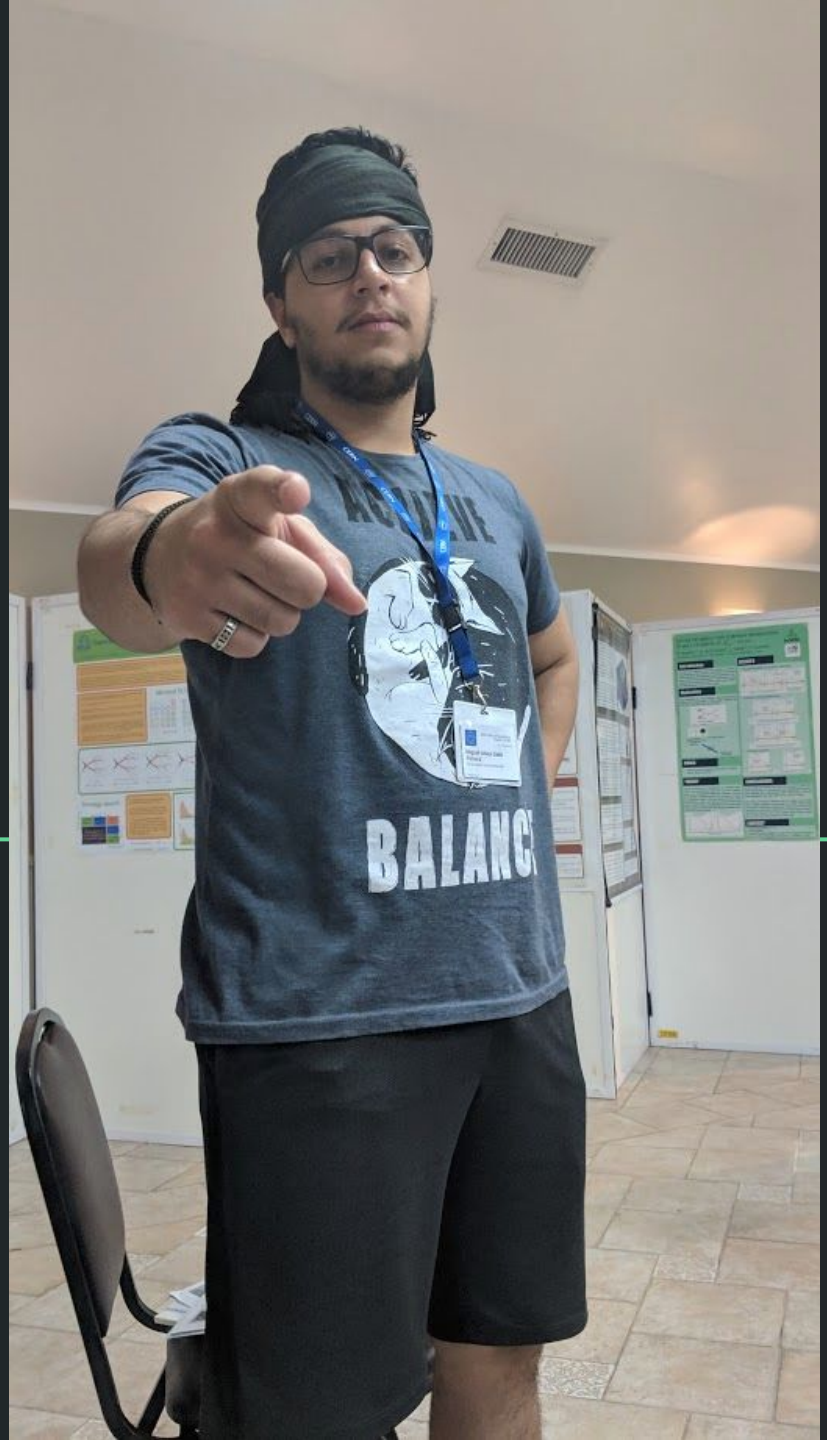
BALANC

Heitler (superposition) model

$$E = \frac{E_0}{N} \longrightarrow N(X) = 2^{\frac{X}{\lambda}} = \frac{E_0}{E(X)}$$

E_0 = primary energy, E = Energy per particle
λ = interaction depth

$$N(X_{max}) = N_{max} = 2^{\frac{X_{max}}{\lambda}} = \frac{E_0}{E_c}$$

At E_c ionization = bremmstrahlung

Bremmstrahlung: radiation produced by deceleration of a charged particle when deflected by another charged particle.

Slant Depth: $X(z) = \int_z^\infty \rho(\mathbf{r}(z'))dz'/cos\, q$

Amount of material transvesed by the shower at *z* position in the axis of the cosmic ray.

$$X(z_{sea-level}) \sim 1000 \frac{g}{cm^2}$$

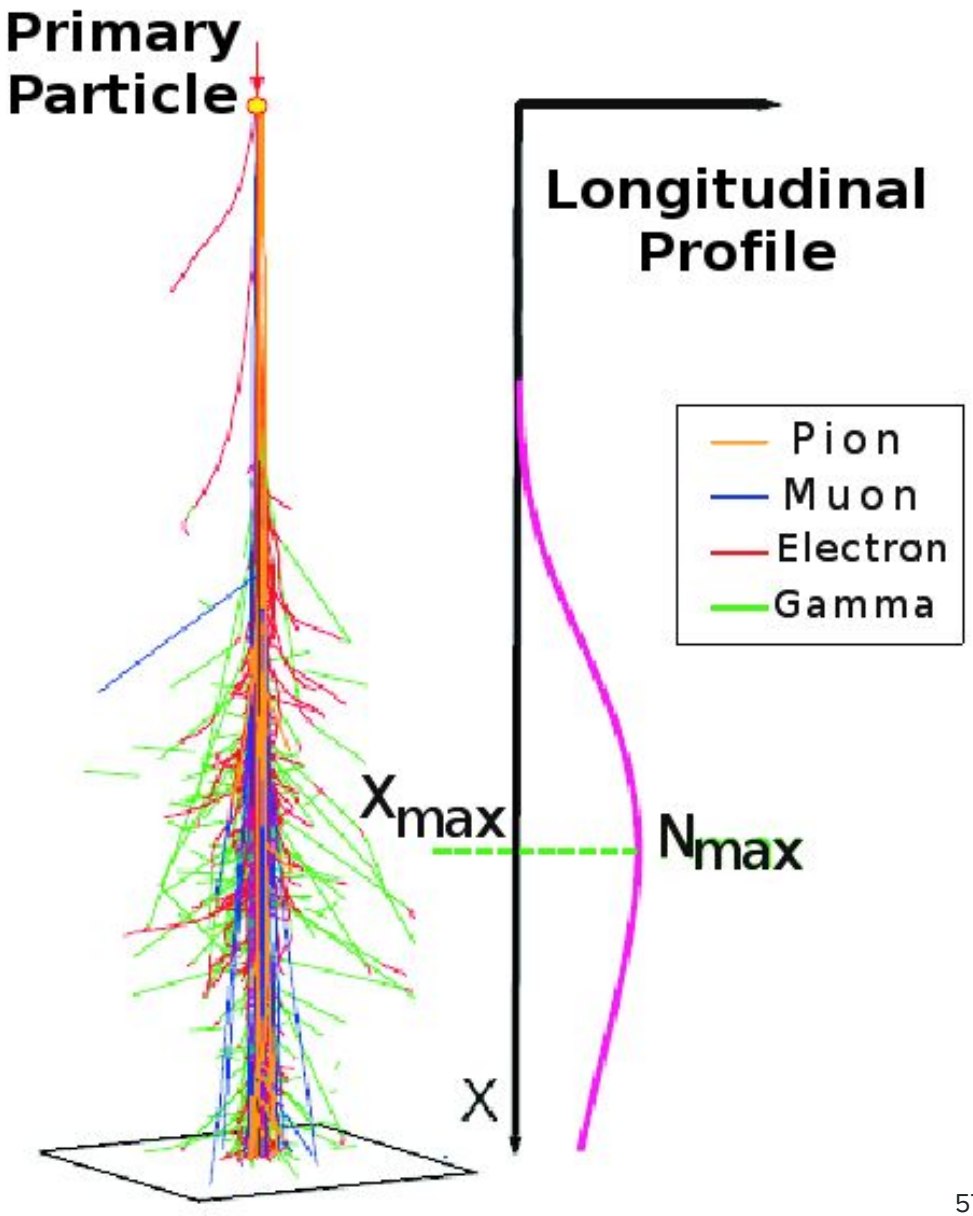

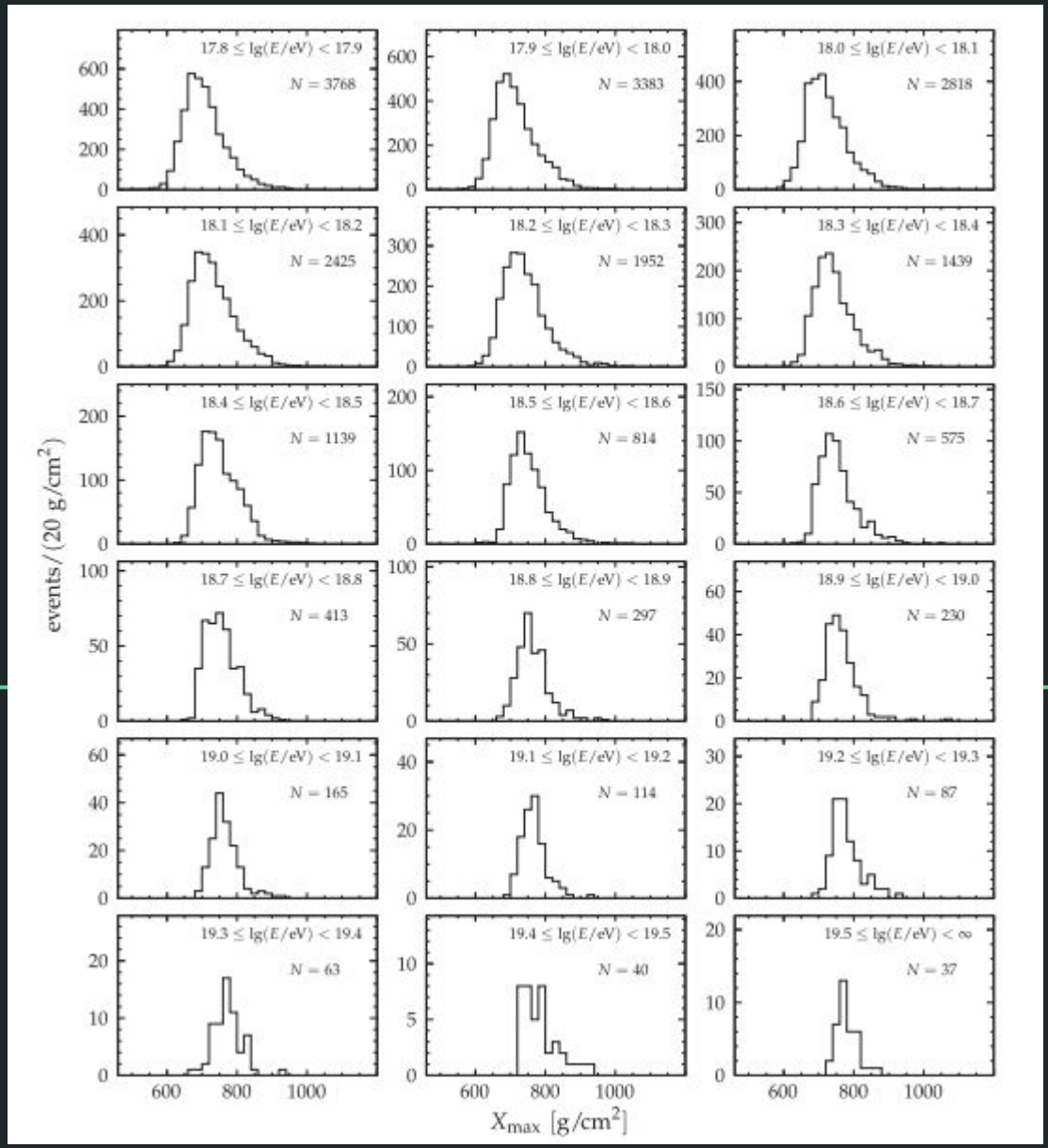
17.8 ≤ lg(E/eV) < 17.9
N = 3768
17.9 ≤ lg(E/eV) < 18.0
N = 3383
18.0 ≤ lg(E/eV) < 18.1
N = 2818
18.1 ≤ lg(E/eV) < 18.2
N = 2425
18.2 ≤ lg(E/eV) < 18.3
N = 1952
18.3 ≤ lg(E/eV) < 18.4
N = 1439
18.4 ≤ lg(E/eV) < 18.5
N = 1139
18.5 ≤ lg(E/eV) < 18.6
N = 814
18.6 ≤ lg(E/eV) < 18.7
N = 575
18.7 ≤ lg(E/eV) < 18.8
N = 413
18.8 ≤ lg(E/eV) < 18.9
N = 297
18.9 ≤ lg(E/eV) < 19.0
N = 230
19.0 ≤ lg(E/eV) < 19.1
N = 165
19.1 ≤ lg(E/eV) < 19.2
N = 114
19.2 ≤ lg(E/eV) < 19.3
N = 87
19.3 ≤ lg(E/eV) < 19.4
N = 63
19.4 ≤ lg(E/eV) < 19.5
N = 40
19.5 ≤ lg(E/eV) < ∞
N = 37
events / (20 g/cm²)
X_max [g/cm²]

❖ Predictions of the moments from simulations for proton and iron induced air showers to the data

- The simulation (CONEX) have been performed using the three hadronic interaction models

EPOS LHC SIBYLL 2.1 QGSJET II 04

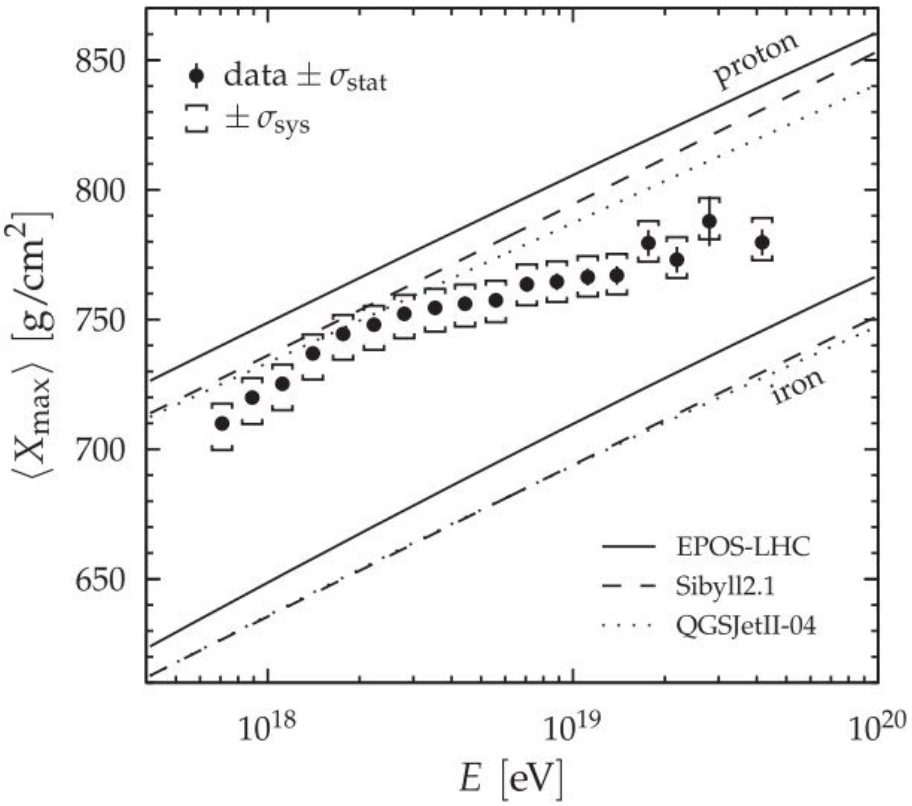

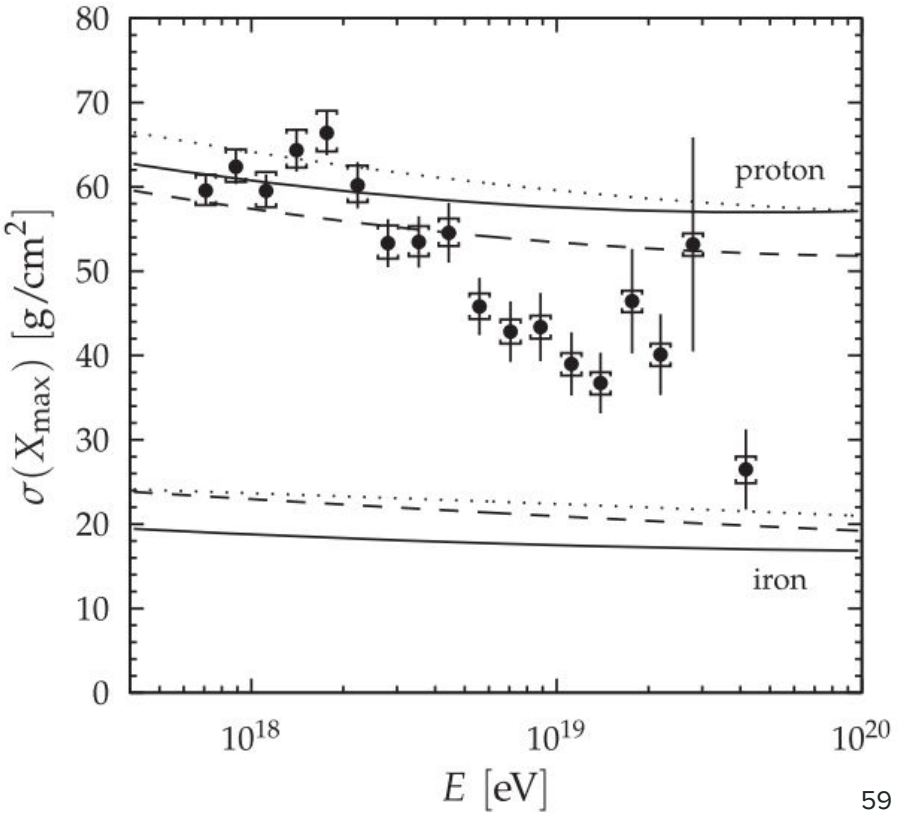

Average of the logarithmic mass and its variance estimated from data using different interaction models

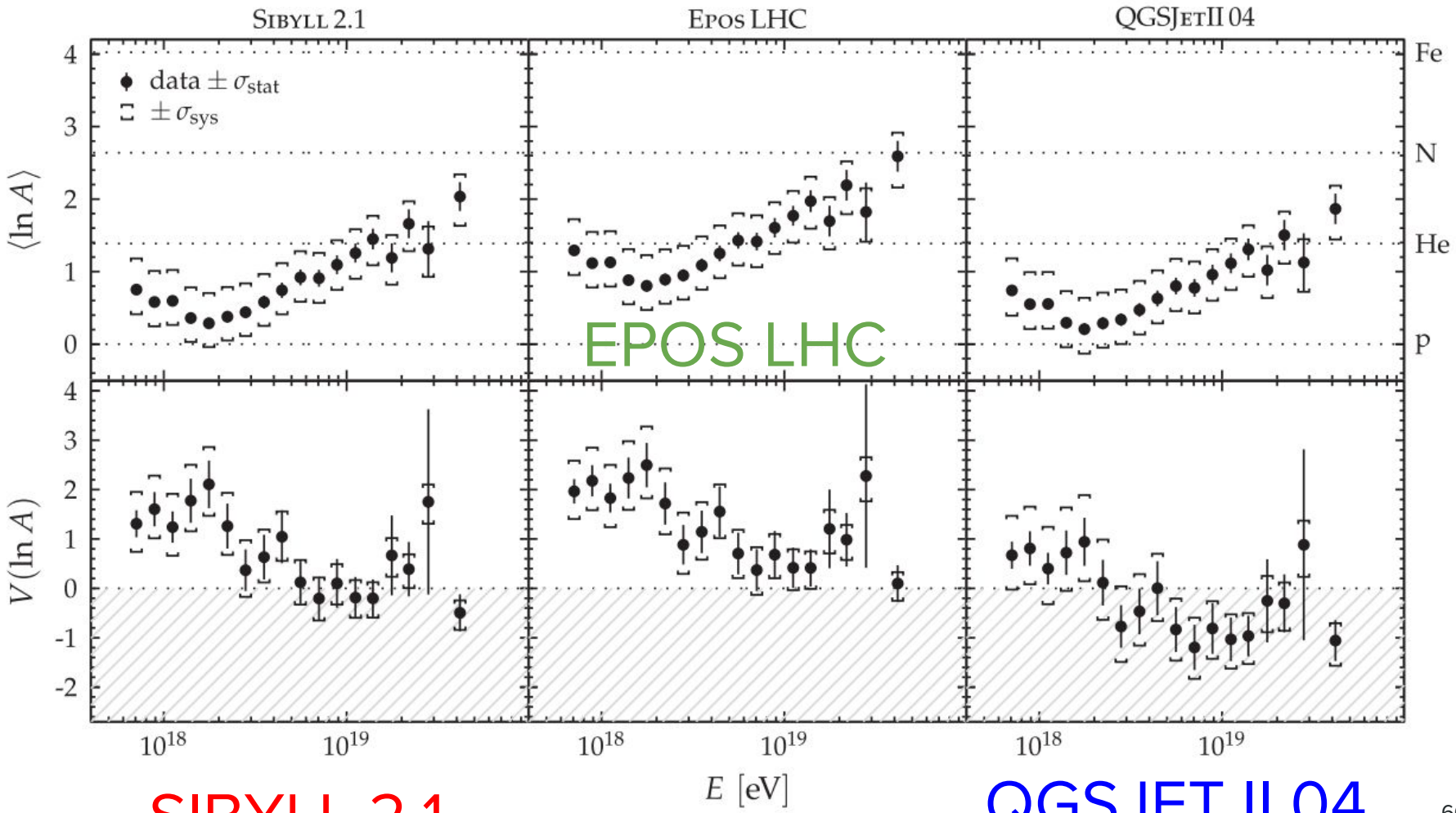

TECH

NASA worried that cosmic rays are going to fry plane passengers' brains

By Margi Murphy, The Sun

January 30, 2017 | 4:14pm | Updated

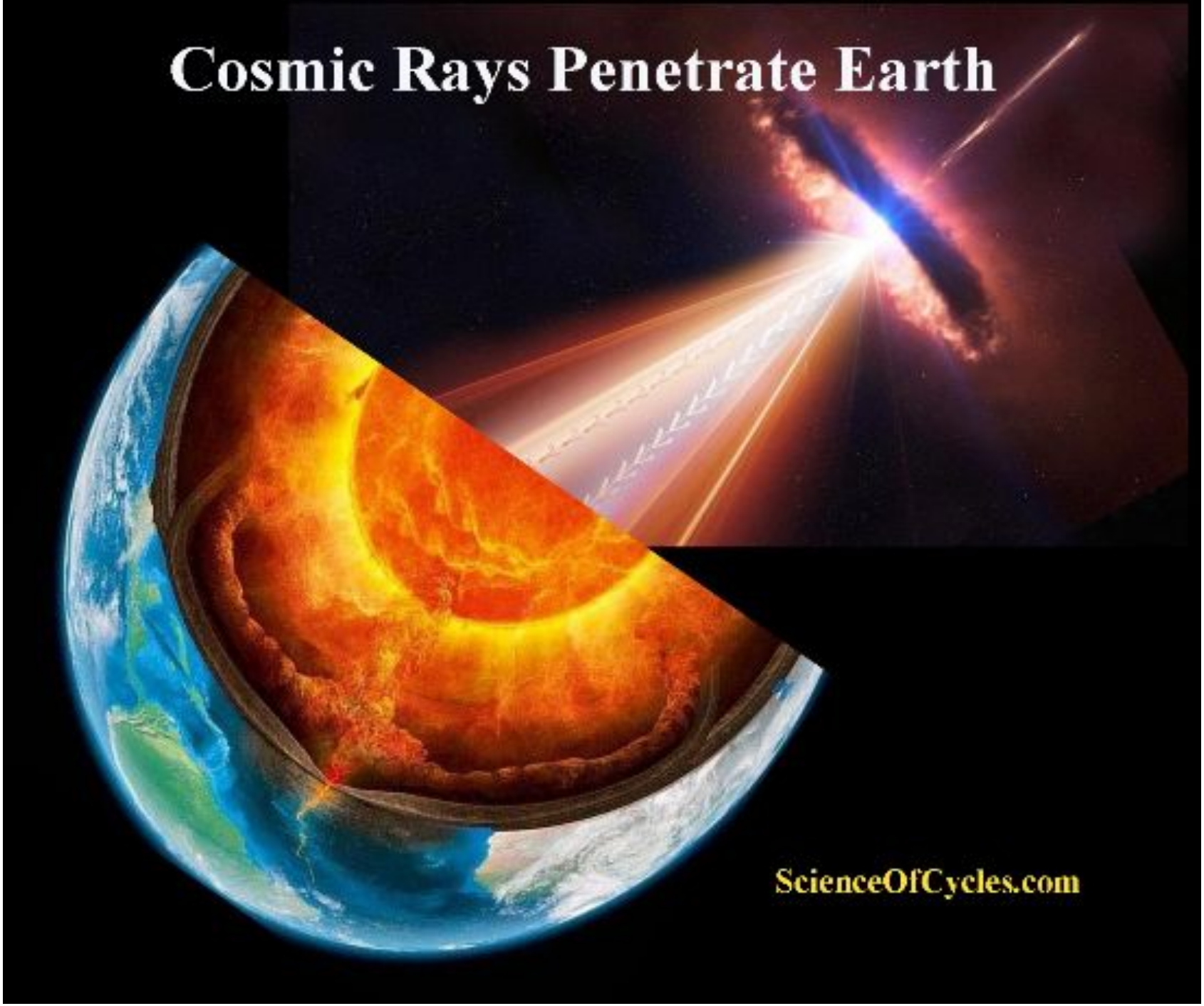
Cosmic Rays Penetrate Earth
ScienceOfCycles.com

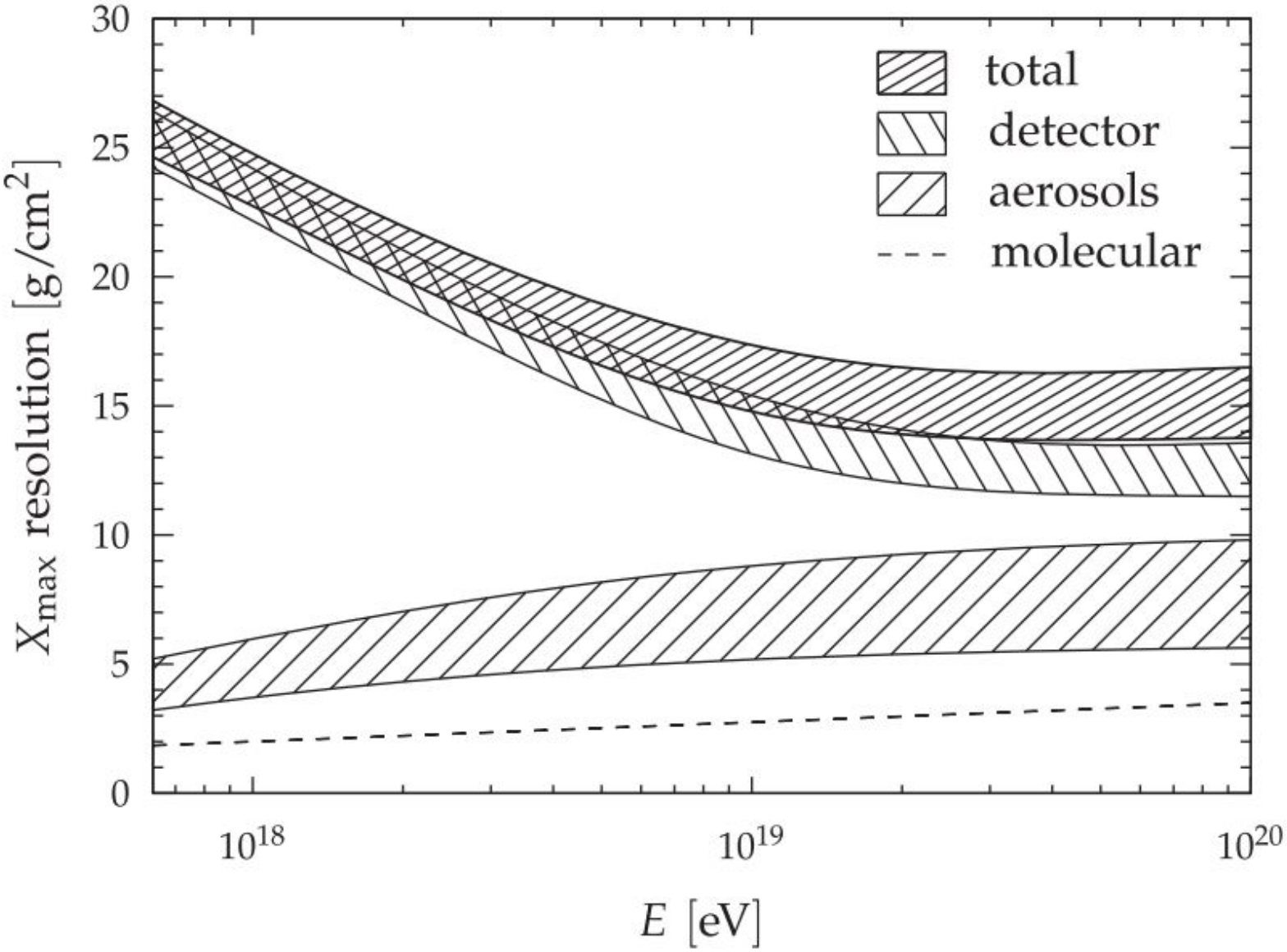

FIG. 6. X_{max} resolution as a function of energy. Bands denote the estimated systematic uncertainties.

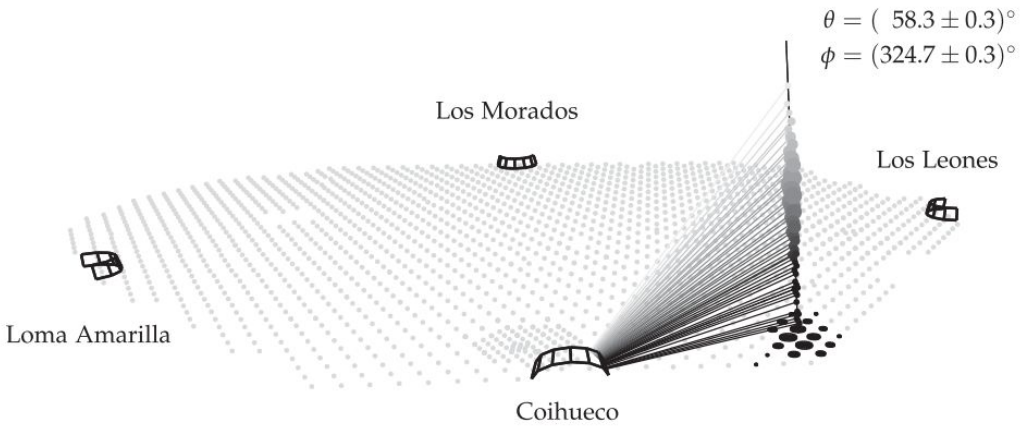

(b) Event geometry. Pixel viewing angles are shown as shaded lines and the shower light and surface detector signals are illustrated by markers of different size in logarithmic scale.

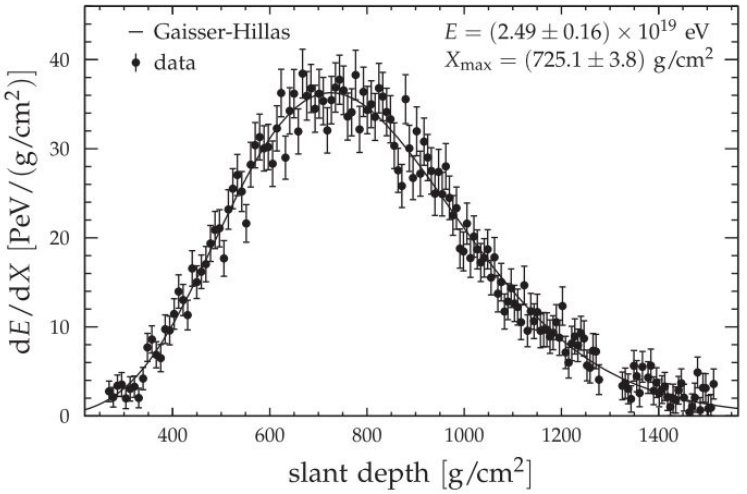

(d) Longitudinal profile (dots) and Gaisser-Hillas function (line).

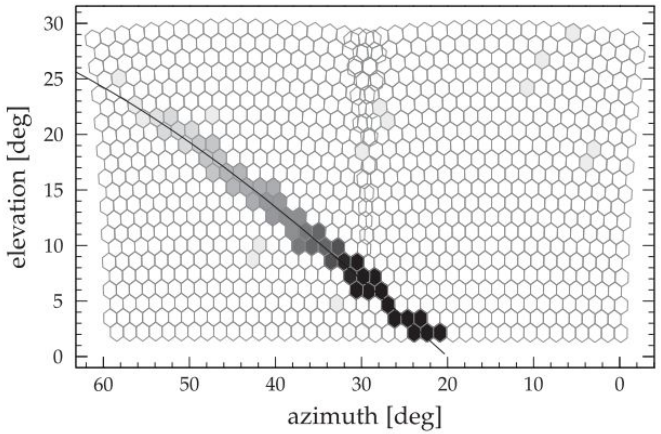

(a) Camera view. The timing of the pixel pulses is denoted by shades of gray (early = light, late = dark). The line shows the shower detector plane.

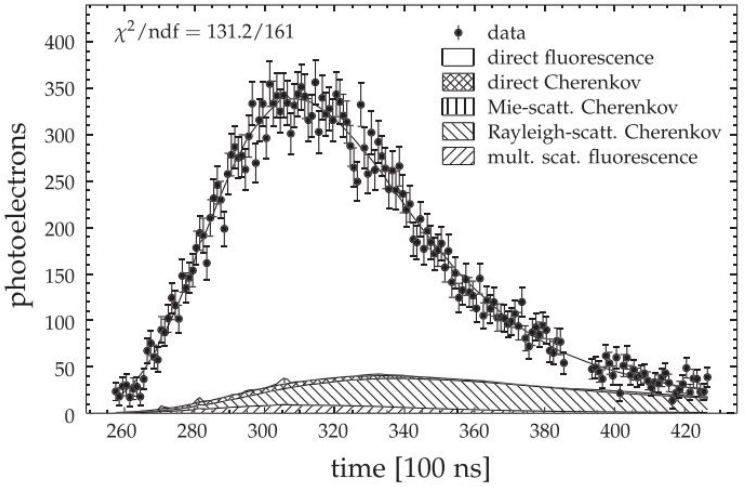

(c) Detected photoelectrons (dots) and the fitted contributions from components of the shower light (open and hatched areas).

Efficiency check (Data and MC)

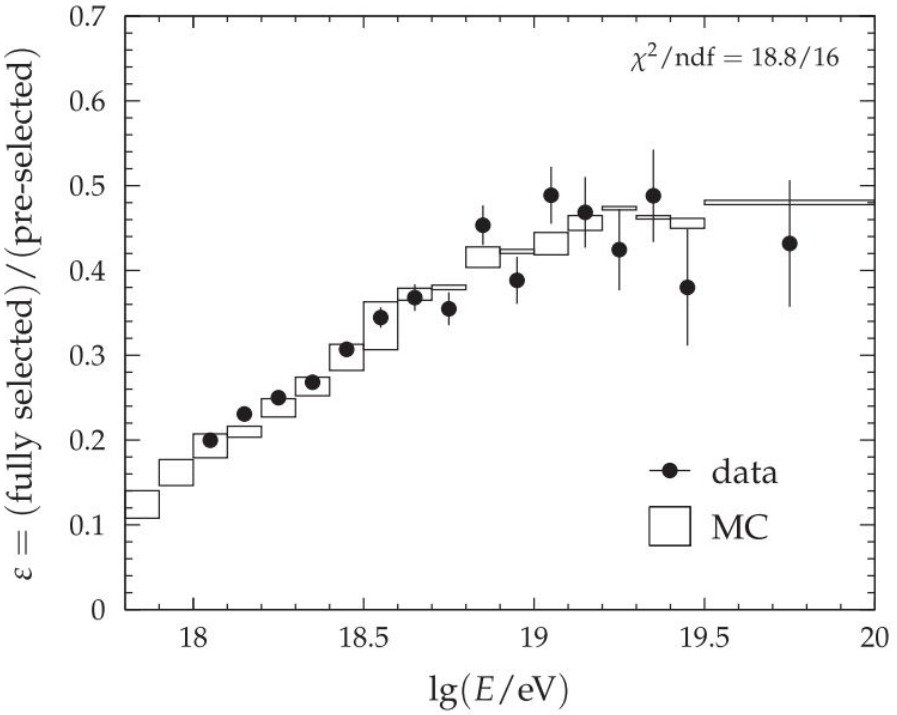

FIG. 8. Efficiency of the quality and fiducial selection for data and Monte Carlo simulation (MC). The χ^2 of the sum of the (data-MC) residuals is quoted on the top right.

Detector resolution cross check between the separate sites

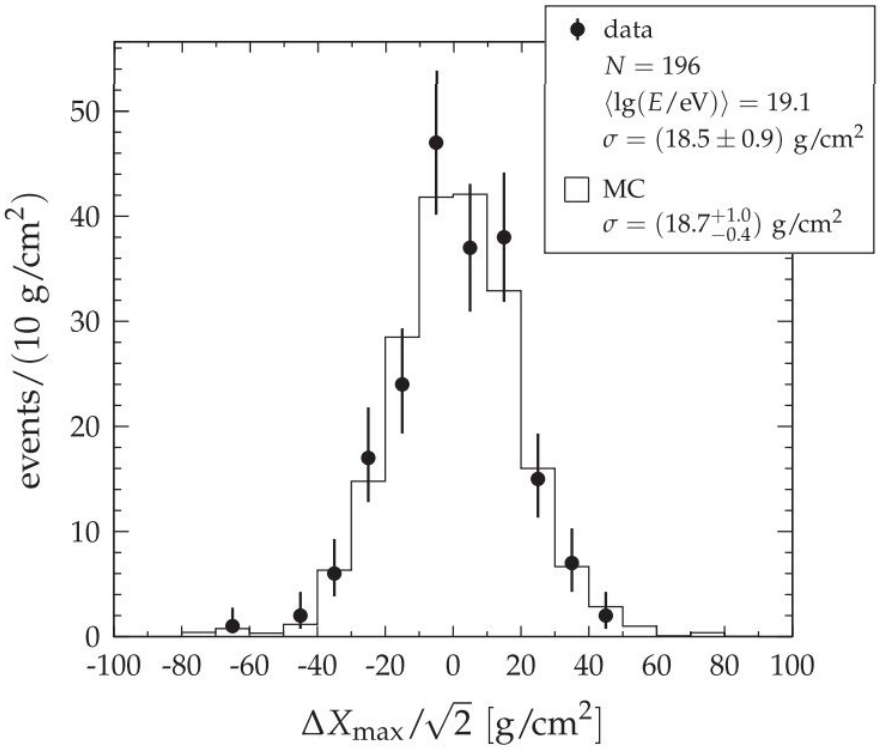

FIG. 9. Distribution of $X_{\max}$ differences for events measured by more than one FD station. The quoted uncertainties for the standard deviation σ are statistical for data and systematic for MC. The latter are dominated by the uncertainty in the contribution of the alignment and aerosols to the resolution (cf. Sec. VI).

Simulated distributions with and without detector effects

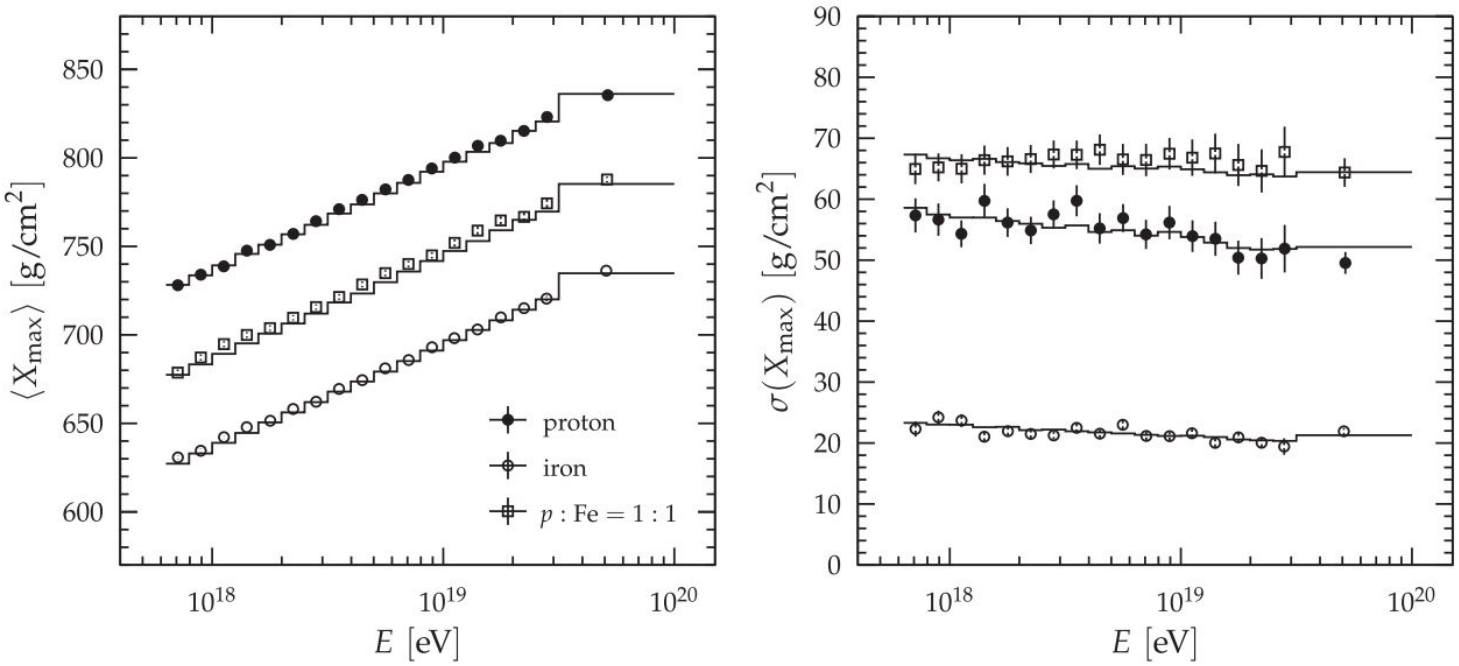

FIG. 10. Reconstructed $\langle X_{max} \rangle$ and $\sigma(X_{max})$ (symbols) obtained from simulated data for different compositions using the SIBYLL2.1 interaction model. The moments of the generated events before detector simulation are shown as solid lines.

Cross-Check Summary

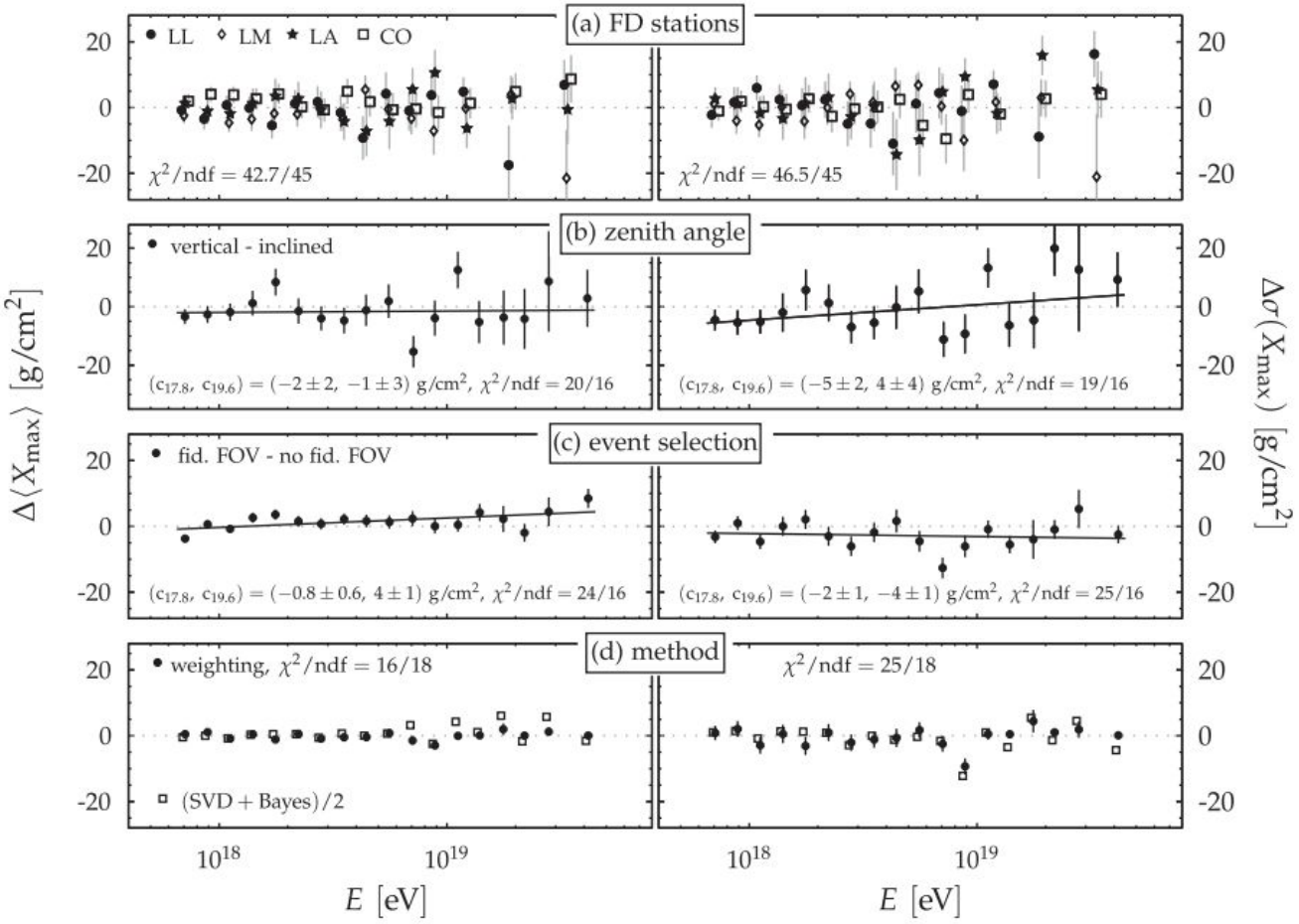

FIG. 11. Cross-checks. (a) Difference of moments obtained from each FD site separately to the results using data from all sites. The global χ^2/ndf with respect to zero is given. (b) Subdivision of the data set in showers with near-vertical and inclined arrival directions. Parameters of a linear fit in $\lg(E)$ are shown with supporting points $c_{17.8}$ and $c_{19.6}$ at the centers of the first and last bin of $10^{17.85}$ and $10^{19.62}$ eV. (c) Difference of results with and without fiducial field-of-view selection. Parameters are the same as in panel (b). (d) Comparison of different methods to estimate $\langle X_{max}\rangle$ and $\sigma(X_{max})$. The difference from the default method is shown. The average from the two deconvolution methods (SVD and Bayesian) is shown without error bars (see text). For the weighting method, the χ^2/ndf with respect to zero is given.

2. Λ_η method

When the shower maxima of the events in the tails of the $X_{\max}$ distribution follow an exponential distribution,

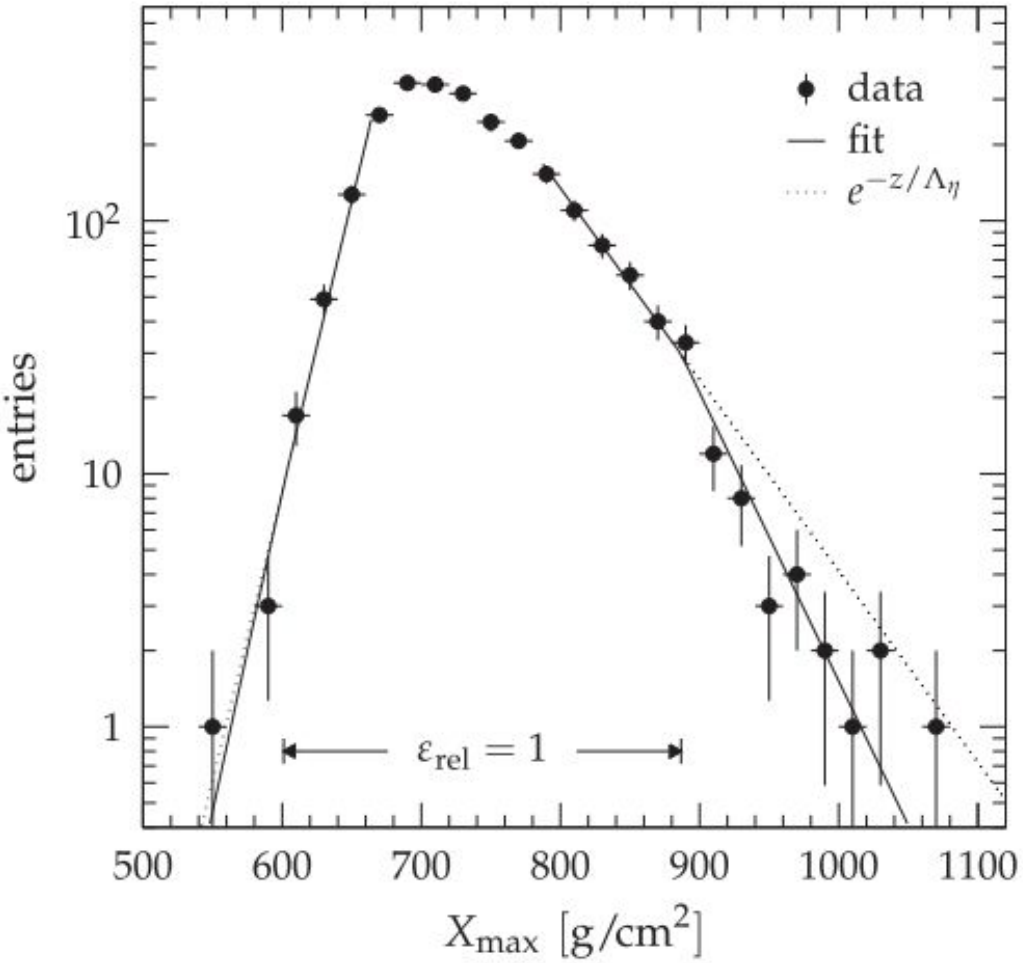

FIG. 15. Fit to the tails of the $X_{\max}$ distribution [$18.1 < \lg(E/\text{eV}) < 18.2$]. The region of constant acceptance $\varepsilon_{\rm rel} = 1$ is indicated by arrows.

Result Summary Table

TABLE III. Parameters of the $X_{\max}$ resolution [Eq. (8)]. σ_1 and σ_2 are in g/cm^2. The uncertainties are systematic and fully correlated between σ_1 and σ_2.

lg E range	σ_1	σ_2	f
[17.8,17.9)	17.5 ± 0.7	33.7 ± 1.4	0.62
[17.9,18.0)	16.7 ± 0.7	32.9 ± 1.4	0.63
[18.0,18.1)	15.9 ± 0.7	31.9 ± 1.4	0.63
[18.1,18.2)	15.1 ± 0.7	31.0 ± 1.4	0.64
[18.2,18.3)	14.4 ± 0.7	30.0 ± 1.4	0.65
[18.3,18.4)	13.8 ± 0.7	29.1 ± 1.5	0.66
[18.4,18.5)	13.3 ± 0.7	28.1 ± 1.6	0.67
[18.5,18.6)	12.8 ± 0.8	27.1 ± 1.6	0.68
[18.6,18.7)	12.3 ± 0.8	26.3 ± 1.7	0.69
[18.7,18.8)	12.0 ± 0.8	25.4 ± 1.8	0.70
[18.8,18.9)	11.7 ± 0.9	24.7 ± 1.9	0.70
[18.9,19.0)	11.5 ± 0.9	24.1 ± 1.9	0.71
[19.0,19.1)	11.3 ± 0.9	23.6 ± 1.9	0.72
[19.1,19.2)	11.2 ± 0.9	23.3 ± 2.0	0.73
[19.2,19.3)	11.1 ± 0.9	23.1 ± 2.0	0.74
[19.3,19.4)	11.1 ± 1.0	23.1 ± 2.0	0.75
[19.4,19.5)	11.1 ± 1.0	23.2 ± 2.0	0.76
[19.5, ∞)	11.2 ± 1.0	23.7 ± 2.1	0.77

TABLE IV. First two moments of the $X_{\max}$ distributions. Energies are in [eV] and $\langle X_{\max} \rangle$ and $\sigma(X_{\max})$ are given in [g/cm^2] followed by their statistical and systematic uncertainties. The number of selected events in each energy bin is given in the third column.

lg E range	$\langle \lg E \rangle$	N	$\langle X_{\max} \rangle$	$\sigma(X_{\max})$
[17.8,17.9)	17.85	3768	$709.9 \pm 1.2^{+7.6}_{-10.2}$	$59.6 \pm 1.7^{+1.9}_{-1.7}$
[17.9,18.0)	17.95	3383	$719.9 \pm 1.4^{+7.5}_{-10.2}$	$62.4 \pm 2.1^{+2.1}_{-1.8}$
[18.0,18.1)	18.05	2818	$725.2 \pm 1.5^{+7.4}_{-10.2}$	$59.5 \pm 2.0^{+2.2}_{-1.9}$
[18.1,18.2)	18.15	2425	$736.9 \pm 1.8^{+7.3}_{-10.1}$	$64.3 \pm 2.6^{+2.4}_{-2.1}$
[18.2,18.3)	18.25	1952	$744.5 \pm 2.0^{+7.3}_{-9.9}$	$66.4 \pm 2.6^{+2.6}_{-2.2}$
[18.3,18.4)	18.35	1439	$748.0 \pm 2.0^{+7.3}_{-9.7}$	$60.2 \pm 2.8^{+2.3}_{-2.0}$
[18.4,18.5)	18.45	1139	$752.2 \pm 2.1^{+7.3}_{-9.4}$	$53.3 \pm 2.9^{+2.1}_{-1.8}$
[18.5,18.6)	18.55	814	$754.5 \pm 2.2^{+7.3}_{-9.1}$	$53.5 \pm 3.0^{+1.9}_{-1.7}$
[18.6,18.7)	18.65	575	$756.1 \pm 2.7^{+7.4}_{-8.8}$	$54.5 \pm 3.5^{+1.7}_{-1.6}$
[18.7,18.8)	18.75	413	$757.4 \pm 2.8^{+7.5}_{-8.5}$	$45.8 \pm 3.4^{+1.5}_{-1.5}$
[18.8,18.9)	18.85	297	$763.6 \pm 2.9^{+7.7}_{-8.1}$	$42.8 \pm 3.6^{+1.4}_{-1.4}$
[18.9,19.0)	18.95	230	$764.6 \pm 3.2^{+7.8}_{-7.8}$	$43.4 \pm 4.1^{+1.3}_{-1.4}$
[19.0,19.1)	19.05	165	$766.4 \pm 3.3^{+8.0}_{-7.6}$	$39.0 \pm 3.8^{+1.3}_{-1.4}$
[19.1,19.2)	19.14	114	$767.0 \pm 3.6^{+8.2}_{-7.4}$	$36.7 \pm 3.6^{+1.3}_{-1.4}$
[19.2,19.3)	19.25	87	$779.5 \pm 5.1^{+8.5}_{-7.2}$	$46.4 \pm 6.2^{+1.2}_{-1.3}$
[19.3,19.4)	19.34	63	$773.1 \pm 5.0^{+8.7}_{-7.1}$	$40.1 \pm 4.8^{+1.3}_{-1.4}$
[19.4,19.5)	19.45	40	$787.9 \pm 9.6^{+8.9}_{-7.0}$	$53.2 \pm 12.7^{+1.3}_{-1.4}$
[19.5, ∞)	19.62	37	$779.8 \pm 5.0^{+9.4}_{-6.9}$	$26.5 \pm 4.8^{+1.5}_{-1.6}$

X_{max} air showers

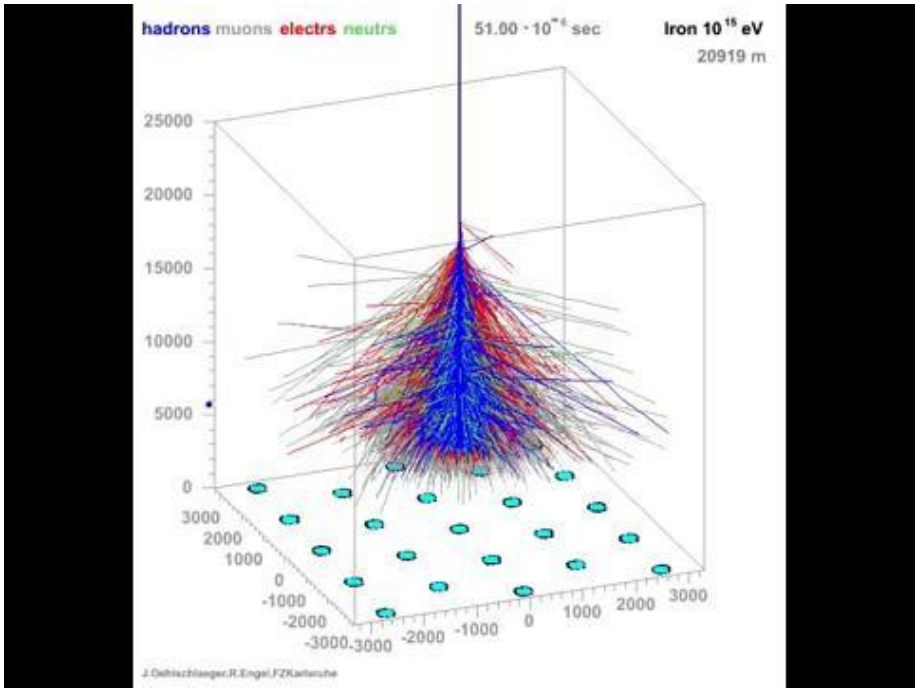

IRON

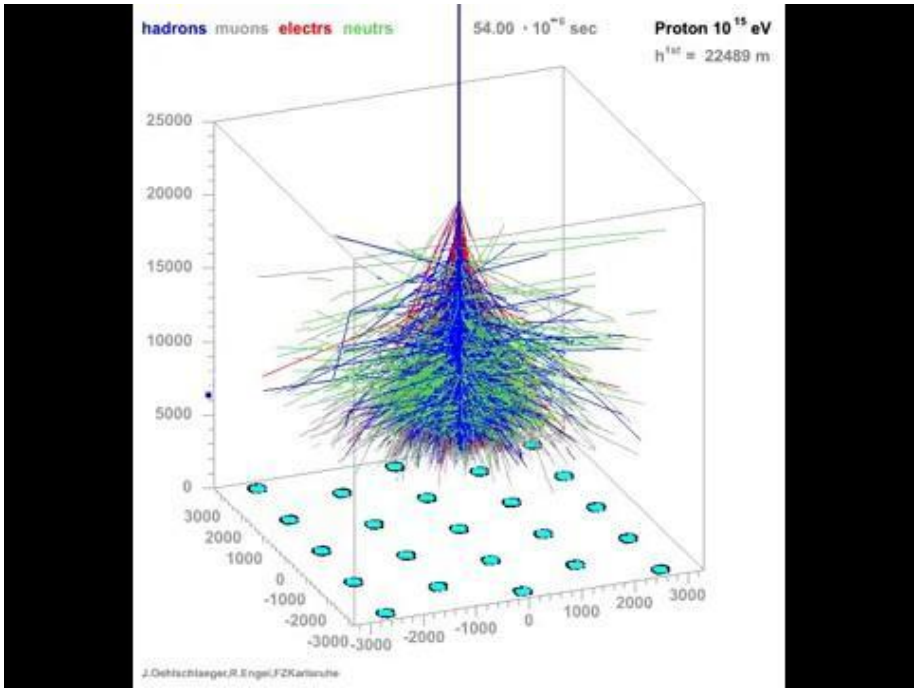

PROTON

https://web.ikp.kit.edu/corsika/movies/Movies.htm

Λ_η method

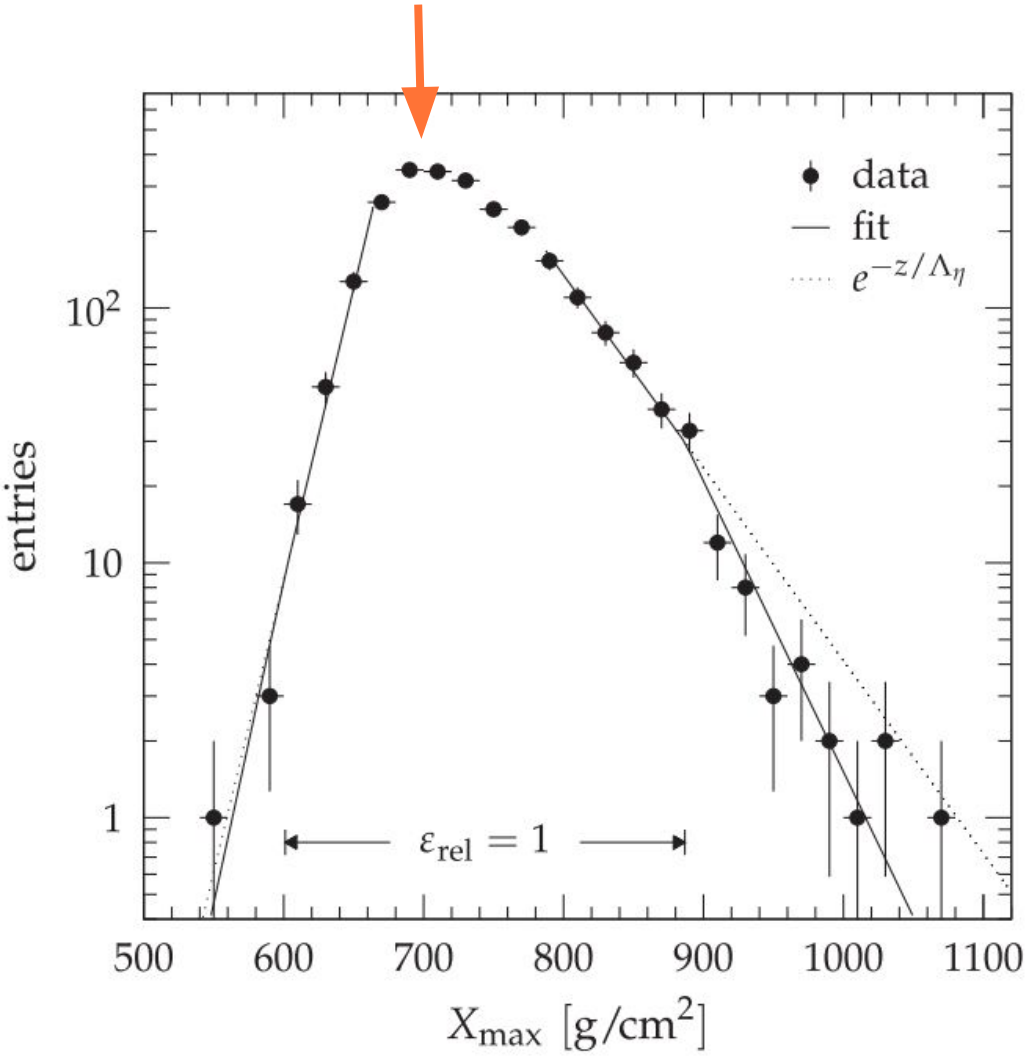

- **Mean and standard deviation of Xmax distribution, <Xmax> and σ(Xmax), respectively.**

  peat

- **For 18.1 < lg(E/eV) < 18.2**

$$< X_{max} >= 736.9 \pm 1.8^{+7.3}_{-10.1}$$

$$\sigma(X_{max}) = 64.3 \pm 2.6^{+2.4}_{-2.1}$$

- **Repeat for other events**

Acceptance is the ratio of selected to generated events

Apply selection criteria to **simulations**

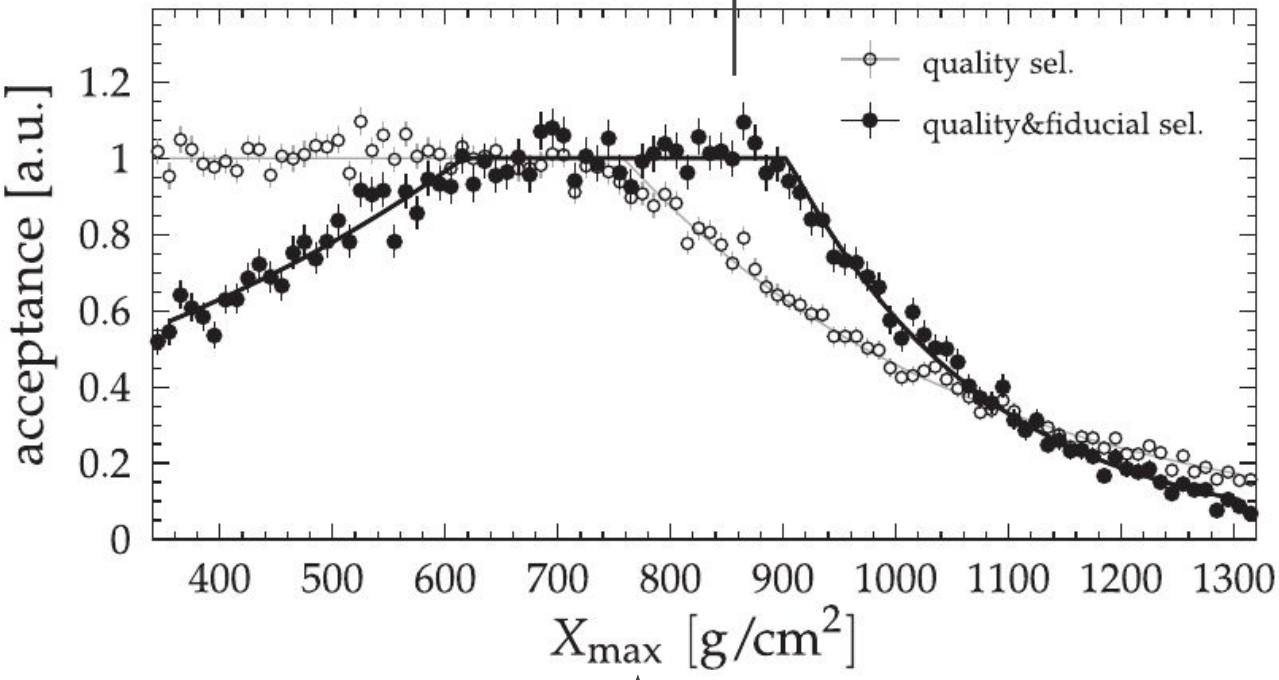

Acceptance depends on X_{max} and E but **not** on the primary

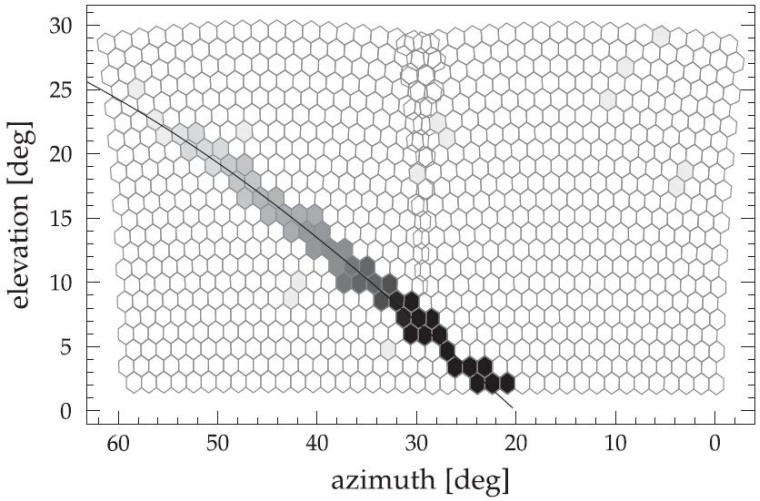

FD detector - Camera View
Early = Light | Late = Dark

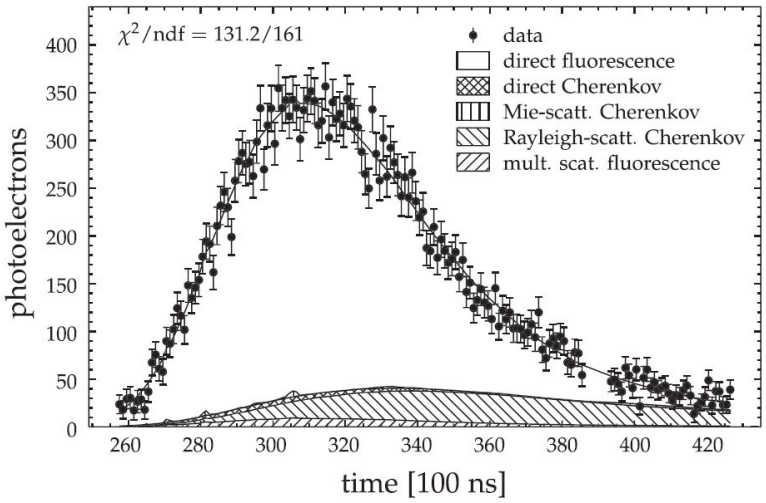

Detected photoelectrons
Time trace of light

Reconstruction

1. Project every time bin to path length $\Delta\ell_i$ at height h_i
2. Estimate the light emitted along $\Delta\ell_i$
3. Light fro cm Cherenkov photons proportional to the energy deposited within the volume
4. Energy deposited proportional to number of particles
5. Fit longitudinal profile to obtain X_{max} and $E(X_{max})$

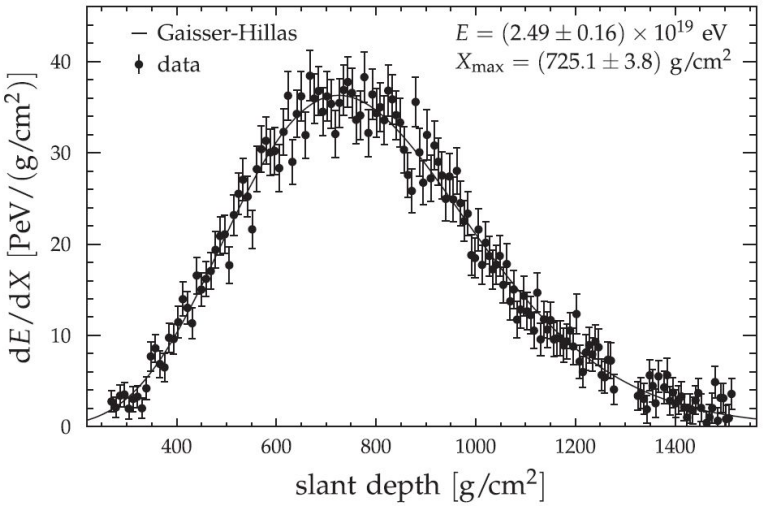

Shower Contains X_{max}

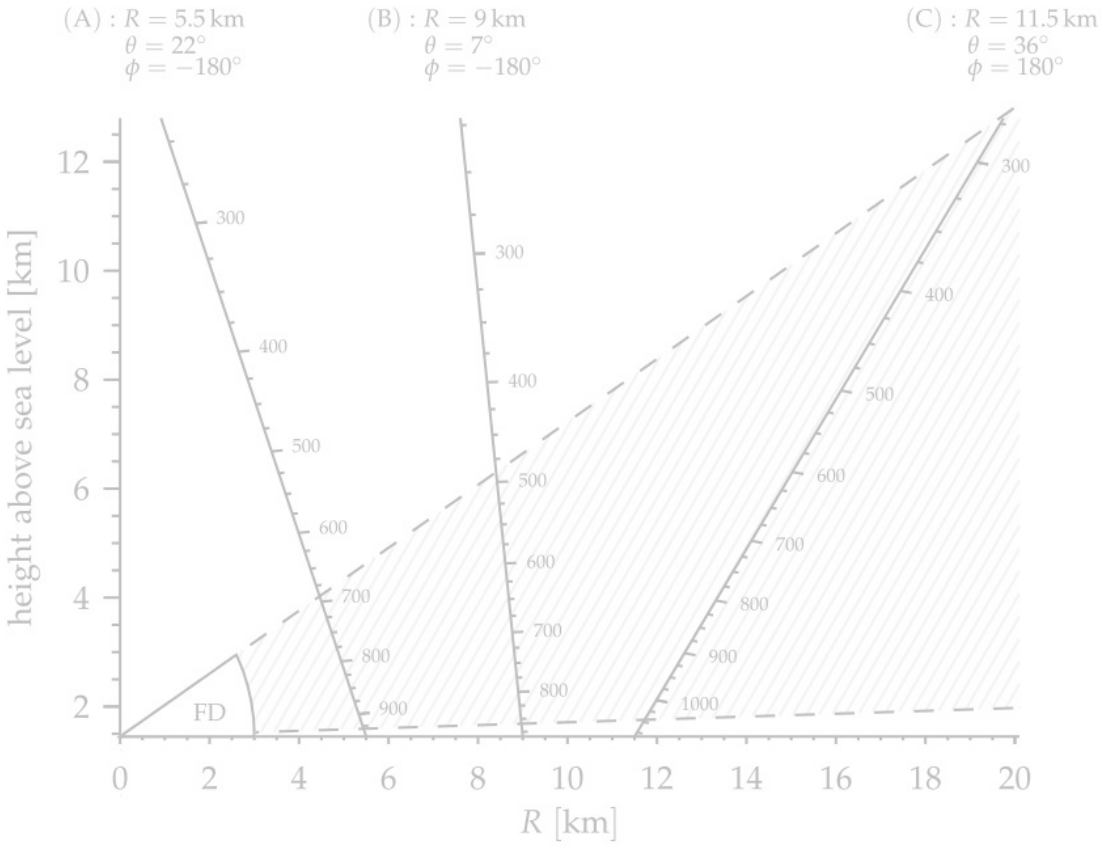

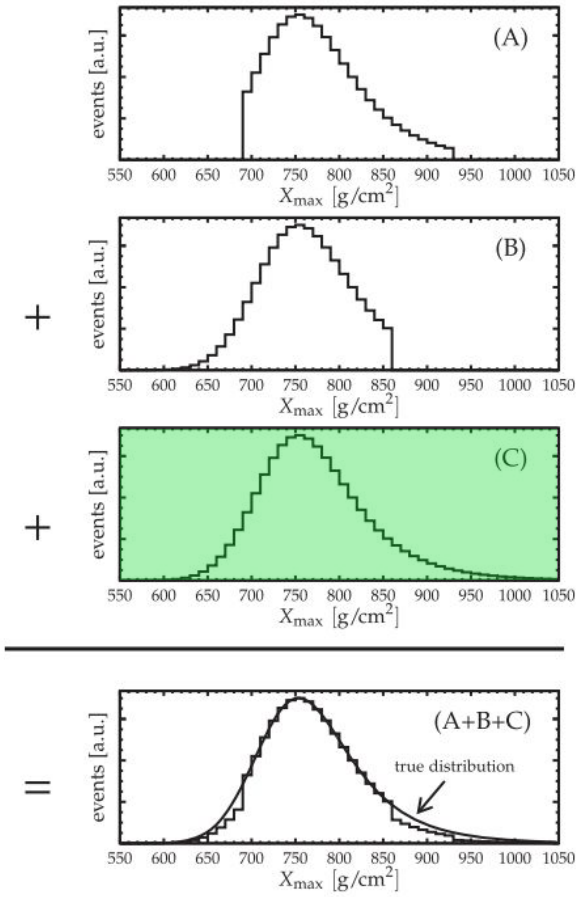

Elongation Rate - **σ**(Xmax)

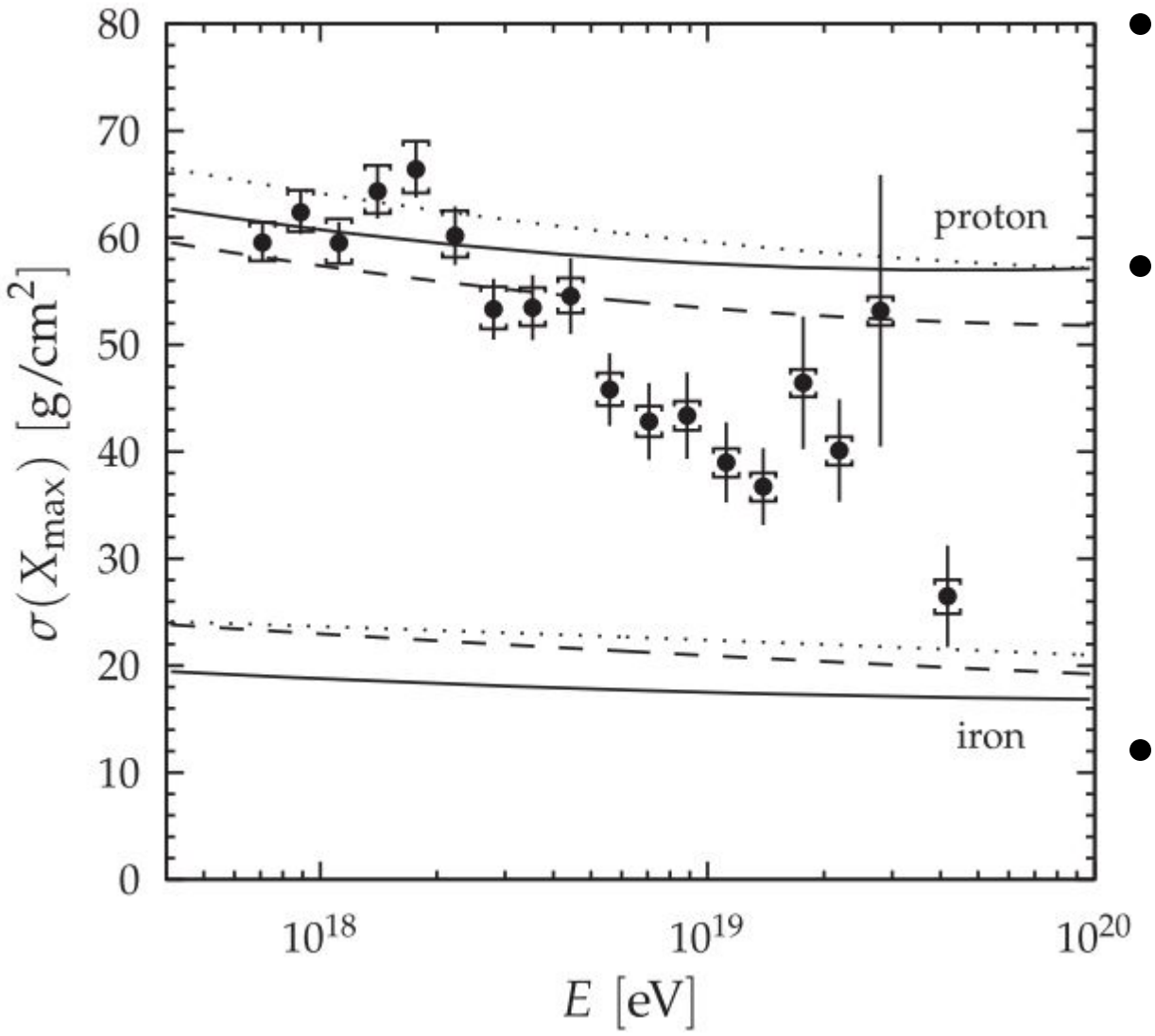

- **Single composition** simulations don't match with data **across** the whole **energy range**
-
  - Divide energy range and define **elongated rate**:

$$D_{10} = \frac{\mathrm{d}\langle X_{\mathrm{max}}\rangle}{\mathrm{d}\lg(E/\mathrm{eV})}.$$

- Changes in **elongated rate** -> change of primary composition

- **Energetic particles** from outer space
- **Primary particle** can be a charged **nucleus** or **gamma** rays
    - Primary interacts with the **atmosphere**, decaying into an **air shower**
    - Leptonic cascade is well modeled, hadronic is model-dependent